

Hopf Bifurcation in Mean Field Explains Critical Avalanches in Excitation-Inhibition Balanced Neuronal Networks: A Mechanism for Multiscale Variability

Junhao Liang^{1,2}, Tianshou Zhou² and Changsong Zhou^{1,3*}

¹Department of Physics, Centre for Nonlinear Studies and Beijing-Hong Kong-Singapore Joint Centre for Nonlinear and Complex Systems (Hong Kong), Institute of Computational and Theoretical Studies, Hong Kong Baptist University, Kowloon Tong, Hong Kong

²School of Mathematics and Guangdong Key Laboratory of Computational Mathematics, Sun Yat-sen University, Guangzhou, P. R. China

³Department of Physics, Zhejiang University, 38 Zheda Road, Hangzhou, China

* Correspondence: cszhou@hkbu.edu.hk

Keywords

E-I balance, Neuronal avalanches, Criticality, Cortical dynamics

Abstract

Cortical neural circuits display highly irregular spiking in individual neurons but variably sized collective firing, oscillations and critical avalanches at the population level, all of which have functional importance for information processing. Theoretically, the balance of excitation and inhibition inputs is thought to account for spiking irregularity and critical avalanches may originate from an underlying phase transition. However, the theoretical reconciliation of these multilevel dynamic aspects remains an open question. Herein, we show that excitation-inhibition (E-I) balanced network with synaptic kinetics can maintain irregular spiking dynamics with different levels of synchrony and critical avalanches emerge near the synchronous transition point. The mechanism is unveiled by a novel mean-field theory that derives the field equations governing the network macroscopic dynamics. It reveals that the E-I balanced state of the network manifesting irregular individual spiking is characterized by a macroscopic stable state, which can be either a fixed point or a periodic motion and the transition is predicted by a Hopf bifurcation in the macroscopic field. Furthermore, these multiscale variable behaviours can be jointly observed in the spontaneous activities of mouse cortical slice *in vitro*, indicating universality of the theoretical prediction. Our theory unveils the mechanism that permits complex neural activities in different spatiotemporal scales to coexist and elucidates a possible origin of the criticality of neural systems. It also provides a theoretical framework for analyzing the macroscopic dynamics of E-I balanced networks and its relationship to the microscopic counterparts, which can be useful for large-scale modeling and computation of cortical dynamics.

Introduction

The mammal brain consists of tens of billions of neurons, which process information and communicate through electrophysiological action potentials, also known as spikes. This large number of neurons exhibits diverse spiking behaviours across broad ranges of spatial and temporal scales [1–3]. Understanding the physical origin and dynamic mechanism of this complexity is crucial for the advancement of neurobiology, the development of therapies for brain diseases and the future design of brain-inspired intelligent systems.

Two striking features can be simultaneously observed at different levels in cortical neuronal systems: 1) irregularity in spiking times, indicated by seemingly random spiking time that resembles Poisson process [4,5] of individual neurons; 2) variability in population firing rates, manifested in widely observed collective neural activities such as population oscillations [6,7] and critical neural avalanches [8–11], etc. Biologically, the spiking irregularity has been proposed to originate from the balance between excitation (E) and inhibition (I) inputs so that spiking of neurons is driven by fluctuations [12–14], and has been associated with functional advantages in efficient coding and information processing [15]. The emergence of collective cortical activities originates in the fact that neurons interact through recurrent networks [16], in which dynamic activities can reverberate. As a result, dynamic correlations arise from structural correlations. In particular, even weak pairwise correlation is sufficient to induce strongly correlated collective network activities [17]. Collective neural activities can emerge with different amplitudes and are often organised as critical avalanches with various sizes [8–11]. These avalanches are cascades of activity bursts in neuronal networks. At criticality, the size and duration of avalanches are approximately distributed according to power-laws, with critical exponents satisfying the scaling relation [18]. Avalanches in the critical state can maximise the informational complexity and variability, and are thought to have functional advantages in information processing [19–21]. However, the mechanism by which E-I balance induced irregular spiking can coexist with critical collective behaviour [10] in recurrent neural circuit remains unclear.

While the traditional mean-field theory of E-I balanced networks [22–24] with binary neuron and instantaneous synapse explains the spiking irregularity of individual neurons, it fails to account for collective neural activities, because it predicts an asynchronous dynamic state with vanishing correlation in unstructured (i.e. random topology) networks. Such vanishing correlation arises due to sparse network connectivity [23] or shared excitatory and inhibitory inputs cancelling correlation in dense recurrent networks [24]. In terms of rate coding, the asynchronous state is not efficient for information processing, as the population firing rate only exhibits a linear response to the input rate [22] but without firing rate variability on faster time scales. In this case, the whole network acts as a rate unit for computation. Under asynchronous dynamics, firing rate variability can arise from heterogeneous neural network structures [25]. For example, clustered network structures [26] can induce slow firing rate oscillations and show stimulus-induced variability reductions. Hierarchical modular networks [27] can support self-sustained firing rate oscillations across different levels. Spatial networks involving a distance-dependent coupling rule can unveil the distance-tuned correlation relation [28,29] and the emergence of propagating waves [30–32] observed in experiments. However, even in unstructured networks, network firing rate oscillations can be induced by realistic synaptic filtering kinetics [6,33]. Such oscillations typically occur in cases where the synaptic decay time scales of inhibition are slower than excitation, which is actually a biologically plausible situation if the synaptic receptors under consideration are AMPA for excitation and GABA for inhibition [34,35]. This is beyond the predictive capacity of traditional E-I balance theory, as it ignores synaptic kinetics. Thus, an extended E-I balance theory that can incorporate the synaptic kinetics is still lacking. Critical avalanches can also rise from neural

dynamics under unstructured network topology [8,21], while its dynamic origin is still controversial. Previous theories have suggested that critical neural avalanches may arise at the edge of a phase transition [9,36] (between a quiescent and active phase [8] or near the onset of synchrony [37,38]). Mechanisms other than criticality that generate avalanches with power-law distribution have also been proposed [39,40]. The emergence of critical avalanches has also been proposed to be closely related to the maintenance of E-I balance [36,41,42]. Nevertheless, the exact relationship between neural criticality and E-I balance and how synchrony can arise in an E-I balanced network, remain poorly understood.

Here, we try to address the above important open questions. We first re-examine the dynamics of integrate-and-fire E-I neuronal network with realistic synaptic kinetics. Mediated by appropriate synaptic time scale, the network can manifest individually irregular spiking activities with different synchronous levels. The network firing rate dynamics can be effectively captured by a set of macroscopic field equations derived by a novel mean-field theory. The synchronous transition point where network firing rate oscillation emerges is predicted by a Hopf bifurcation in the field equations. We find that critical microscopic avalanche dynamics emerges near the onset of synchronization, with critical exponents approximately satisfying the scaling relations, which manifests the hallmark of criticality [43]. The mechanism of critical avalanches could be understood as demographic noise-driven random walks near a macroscopic bifurcation point. On this basis, we propose that the E-I balanced state in the microscopic spiking network corresponds to a stable macroscopic state in the field equations. The asynchronous state, consistent with the traditional theory, corresponds to a stable fixed point, which can be destabilised through a Hopf bifurcation, giving rise to a stable limit circle, corresponding to network firing rate oscillation. As such, we theoretically extend the E-I balanced state to incorporate network oscillation with different synchronous levels to account for the coexistence of variability in both individual and population scales. As a primary test of the theory, we empirically verify the coexistence of irregular spiking and collective critical avalanches in the public experimental data of spontaneous spiking activities recorded in mouse somatosensory cortex *in vitro* [44]. Scaling relations similar to the network model are also found to hold in these critical data sets. The theory proposed here explains how collective neural activities coexist with irregular neuron spiking and reveals a possible origin of criticality in neural systems. It also serves as a novel analytical tool to study the dynamics of IF networks with biologically realistic synaptic filtering kinetics, thus can be used in large-scale modeling of brain networks.

Results

Network synchrony arises from loose temporal balance

Consider a homogeneous E-I balanced network modelled by IF neurons with sub-threshold membrane dynamics:

$$\frac{dV_i}{dt} = f_\alpha(V_i) + J_{\alpha O} \sum_{j \in \partial_i^\alpha} F^E * s_j(t) + J_{\alpha E} \sum_{j \in \partial_i^\alpha} F^E * s_j(t) + J_{\alpha I} \sum_{j \in \partial_i^\alpha} F^I * s_j(t), \quad (1)$$

where, $V_i(t)$ is the membrane potential of neuron i (belonging to type $\alpha = E, I$) at time t . ∂_i^α represents the α neighbours of neuron i . The input sources for neurons include excitatory inputs from external neurons (population O), inputs from recurrent excitatory neurons (population E)

and inputs from recurrent inhibitory neurons (population I). The first term $f_\alpha(V_i) = (V_{rest}^\alpha - V_i) / \tau_\alpha$ describes intrinsic leaky membrane dynamics and $J_{\alpha\beta}$ are synaptic weights. $s_j(t) = \sum_n \delta(t - t_j^n)$ denotes the spike train of the j -th neuron and it is convoluted with $F^\alpha(t)$, a bi-exponential function:

$$F^\alpha(t) = \frac{1}{\tau_d^\alpha - \tau_r} [\exp(-\frac{t}{\tau_d^\alpha}) - \exp(-\frac{t}{\tau_r})], t \geq 0. \quad (2)$$

where τ_r is the synaptic rise time, and the synaptic decay times τ_d^α , $\alpha = E, I$ depend on the type of presynaptic neuron (see *Materials and Methods* for the details and parameter settings of the model). This synaptic filtering effect plays a non-trivial role in shaping the network dynamics [6,33]. In traditional theory, E-I balance is a case of inhibition domination, in which network inhibitory feedback can cancel the excitatory current spill on a fast time scale (Fig. 1G). Such a ‘strict balance’ holds for fast inhibition decay time and the network spiking dynamics is asynchronous, as shown in Fig. 1C.

This scenario of strict balance breaks down when inhibition becomes slow, which induces an effective delay in the inhibitory cancellation (Fig. 1H). Such a delay before the cancellation would induce a window during which excitatory current spills over the network, resulting in the collective spiking shown in Fig. 1D. The strength of the collective activity depends on the length of this excitation-dominant window. As inhibition becomes dominant again after a delay, a temporal quiescent episode ensues after the collective spiking. In this ‘loose balance’ scenario, the network maintains balance on a slower time scale. In this case, as excitation and inhibition dominate alternately, the strict balance is temporally broken on a fast time scale. Note that in the loose balance state, the delay in the inhibitory cancellation is merely a few milliseconds (Fig. 1H), well consistent with the inhibition tracking delays observed in experiments [14].

These different collective behaviours can be seen from the network firing rate dynamics. The network firing rate in the strict balance asynchronous state is almost steady (Fig. 1E), whereas the loose balance induces firing rate oscillation (Fig. 1F), with fast firing rate variability at the population level. The emergence of oscillation implies a regularity of the population dynamics of the network. However, it is important to stress that the spiking of the neurons is still highly irregular. There are at least two reasons for this irregularity. First, the population oscillation is quasi-periodic rather than periodic due to the stochastic nature of the network dynamics. Second, and more importantly, each collective burst is randomly participated in by partial neurons, referring to Fig. 2E. This can also be understood from the fact that the firing rate is still low at the peaks of spiking activity corresponding to spiking synchrony (Fig. 1F). The histogram counts of the coefficient of variance (CV) of the inter-spike intervals (ISIs) of neurons (see *Materials and Methods*) in the network are shown in Fig. 1I to L. In both asynchronous and synchronous states, the overall value of the CV is around 1, indicating that the spiking irregularity approximately resembles the Poisson process, as confirmed by experimental measurements [4].

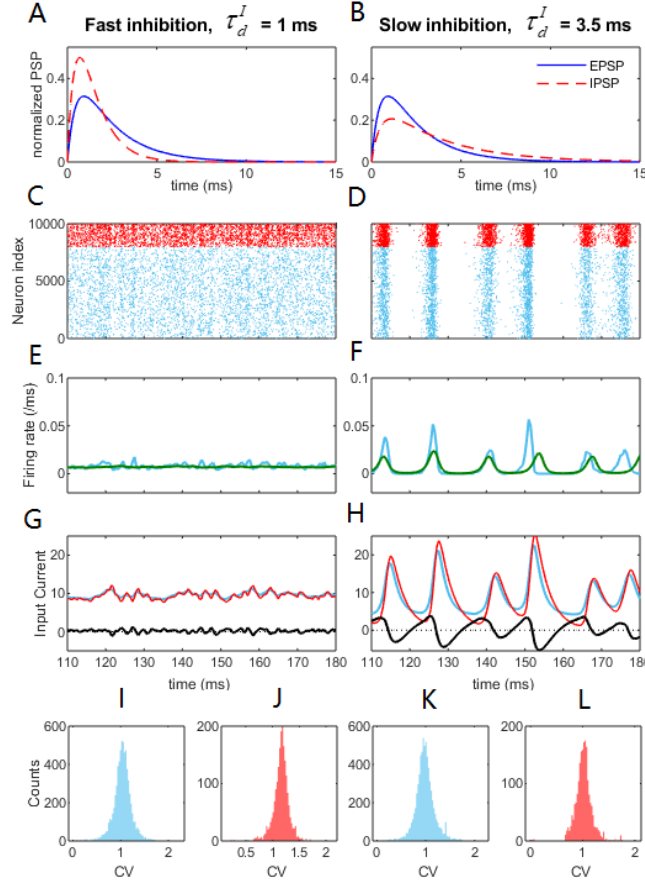


Fig. 1. Synchronisation and network oscillation induced by slow inhibition in balanced networks ($N = 10000$). Fast inhibition (left) induces strict balance with asynchronous spiking and an almost steady network firing rate. Slow inhibition (right) results in loose balance, with synchronous grouped spiking and network oscillation. Individual neurons spike irregularly in both cases. (A, B): Normalised E/I post-synaptic response when receiving a pre-synaptic spike. (C, D): Raster plot of the spiking time. Each blue/red point corresponds to a spike of the E/I neuron. (E, F): The corresponding firing rate of E population (blue) and the firing rate predicted by the field equations (green). (G, H): The blue/red curves represent the average input E/I current of a neuron in the network and the black curves represent the difference between them. (I, J): The histogram counts of the CV of ISI of E neurons (I) and I neurons (J) in the fast inhibition case. (K, L): The same as (I, J) but for the slow inhibition case. The parameters are set as $Q_o = 5 \text{ Hz}$; $\tau_d^I = 1 \text{ ms}$ in the fast inhibition case (left) and $\tau_d^I = 3.5 \text{ ms}$ in the slow inhibition case (right).

Mean-field theory predicts the transition from the irregular asynchronous to the irregular synchronous state

The network dynamic transition induced by a looser E-I balance can be characterised by the dynamics of population firing rate (Fig. 1 E and F). However, an effective theory that can predict the population dynamics of IF networks with synaptic kinetics is still lacking. Here, we propose a

novel mean-field approximation theory to derive the macroscopic dynamic equations of an IF network (details in *Materials and Methods*). The population average firing rate of α type neurons at time t , $Q_\alpha(t)$, is expressed by

$$Q_\alpha(t) = \frac{1}{1 + \exp(\frac{V_{th} - V_\alpha}{\sigma_\alpha} \frac{\pi}{3})}, \quad (3)$$

where $V_\alpha = \langle V_i \rangle_{i \in \alpha}$ are the population-averaged membrane potentials and σ_α are effective parameters representing the standard deviation of the membrane potential. The field equations take the form:

$$\frac{dV_\alpha}{dt} = f_\alpha(V_\alpha) + J_{\alpha o}(n_o Q_o + \sqrt{n_o Q_o / N_\alpha} \xi_\alpha(t)) + J_{\alpha E} \Phi_E + J_{\alpha I} \Phi_I, \quad \alpha = E, I \quad (4)$$

$$(\tau_d^\alpha \frac{d}{dt} + 1)(\tau_r \frac{d}{dt} + 1)\Phi_\alpha(t) = n_\alpha Q_\alpha(t), \quad \alpha = E, I, \quad (5)$$

where $\Phi_\alpha(t) = \left\langle \sum_{j \in \theta_\alpha^i} F^\alpha * s_j(t) \right\rangle_{i \in E, I}$ is the averaged synaptic time course of α inputs received by a neuron, N_α is the number of α neurons, n_α is the average number of α neighbours of a neuron in the network, and $\xi_\alpha(t)$ are independent Gaussian White noise terms. Eqs. (4, 5) provided an effective description of the macroscopic dynamics of the spiking neuronal network Eqs. (1, 2). This technique for deriving the macroscopic field equations is highly generalizable. Extensions to the cases of time-varying inputs and conductance-based dynamics are presented in *Appendix I. Model Extensions*.

The mean firing rate of the network can be estimated from the field equations. Fig. 2A shows the results with different external input strengths and network sizes. It correctly predicts the linear response to external input, a property of asynchronous balanced network [22]. The dynamic difference between the asynchronous state and synchronous state can already be predicted at this point by the field equations in terms of the population firing rate dynamics, as shown in Fig. 1 E and F. The mechanism is explained by a Hopf bifurcation in the field equations through stability analysis (see *Materials and Methods* for further details), as shown in Fig. 2B. In the case of fast inhibition, the fixed point of the field model is generally a stable focus, whose Jacobian has complex eigenvalues with negative real parts. In this case, the network firing rate only fluctuates mildly due to noise perturbations. When τ_d^I increases, the fixed point will lose its stability through a supercritical Hopf bifurcation, as indicated by a pair of its dominant complex conjugate eigenvalues $\lambda = \alpha \pm i\omega$ crossing the imaginary axis. The Hopf bifurcation predicts that the stable fixed point will give way to a stable periodic solution, whose amplitude grows from zero. The frequency of the periodic motion can be estimated as $\omega / 2\pi$ in the linear order. This prediction is approximately equal to the numerically measured peak frequency of the network oscillation near the critical bifurcation point, as shown by the blue circles in Fig. 2B.

As shown in Fig. 2C, the network synchrony increases dramatically after τ_d^I crosses the Hopf bifurcation point. Fig. 2D shows that the network temporal firing rate variability (see *Materials and Methods* for further details) increases conspicuously during this transition, which is also predicted

by the field equations. The CV of ISIs averaged over the excitatory population is shown in Fig. 2E. During the onset of collective oscillation, the averaged CV of ISIs first slightly decreases and then increases (as the bursting oscillation activity develops at around $\tau_d^l \approx 4$ ms, referring to Fig. 3A bottom panel) while its overall value is around 1. The coexistence of irregular spiking and collective oscillation can be understood from the ratio between the mean firing rate of neurons and peak frequency of network oscillation. If each oscillation is participated by all the neurons, then the ratio should approach one. However, as can be seen from Fig. 2E, this ratio is nearly 0.1 after oscillation onset, implying that each oscillation is randomly participated by almost 10% of the neurons, thus each neuron only spikes sparsely and randomly participates in about 10% of the collective oscillations. As τ_d^l further increases to bursting onset, this ratio rapidly increases to approaching one, implying that almost all the neurons participate in each oscillation in the bursting state, where the inhibitory feedback is too slow such that the excitatory current can spill over the whole network in the excitatory dominant period. In addition to spiking time variability, we further examine another branch of irregularity: the fluctuations of firing rate [45,46]. As shown in Fig. 2F, the change of Fano Factor (FF) of the individual neurons (see *Materials and Methods* for further details) is similar to that of CV (Fig. 2E), indicating that the individual firing rate fluctuation does not increase with the onset of collective synchrony. Before the bursting oscillation onset, the value of FF is slightly larger when measured by a larger time window given that the window size is still smaller than the average ISIs of the neurons. When bursting oscillation fully develops, a larger time window will capture the oscillating regularity, resulting in a smaller FF. For time windows ~ 100 ms, the overall individual FF around 1~2 is similar to experimental measures [45,46]. In contrast, the change of population FF (Fig. 2G, and see *Materials and Methods* for details) is similar to the spiking correlation (Fig. 2C) and temporal variability of firing rate (Fig. 2D). This trend was further confirmed by the field model prediction, as shown in Fig. 2H. Thus, it appeared that the observed collective oscillation is a network property rather than an individual neuron property. Hence, the network collective oscillation activity is compatible with individual neuron irregular spiking [47]. The latter property is the prominent feature that the original E-I balance theory has attempted to explain [48].

In summary, strict balance with asynchronous network spiking is predicted by a stable focus and loose balance with synchronous network spiking is predicted by a stable limit circle in the field equations. Both strict and loose balance conditions support the irregular spiking of individual neurons.

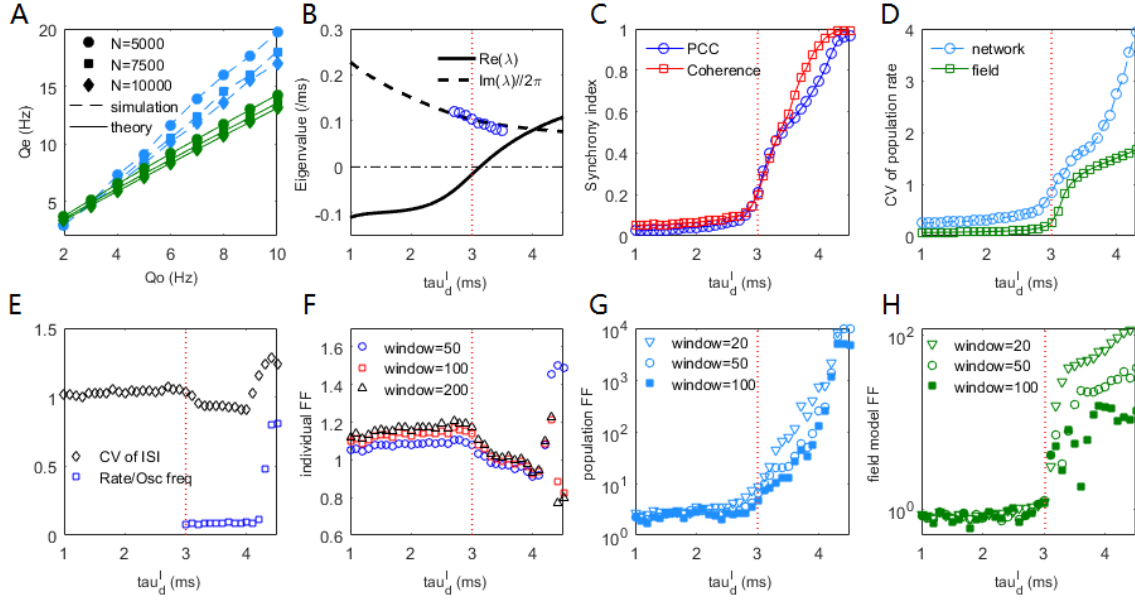


Fig. 2. The mean-field theory prediction of the dynamic transition of the spiking network. (A) The excitatory firing rate in the asynchronous steady-state ($\tau_d^I = 1 \text{ ms}$) under different strengths of external input and different network sizes. Theoretical results (green solid lines) are obtained from field Eqs. (4, 5). Synaptic strengths $J_{\alpha\beta}$ are multiplied by 1.41 and 1.15 in the cases of $N = 5000$ and $N = 7500$, respectively to maintain the usual scale $J_{\alpha\beta} \sim N^{-1/2}$. (B) Deterministic field equations predict that a Hopf bifurcation occurs with the increase of inhibitory decay time τ_d^I at a critical value around $\tau_d^I \approx 3 \text{ ms}$ (indicated by a vertical dashed line). The real part and imaginary part divided by 2π of the dominant eigenvalue are denoted by the solid and dashed lines, respectively. Blue circles are peak frequencies of the excitatory firing rate oscillation from network simulation. (C) The PCC and coherence index show the emergence of network oscillation as τ_d^I increases. (D) The CV of population firing rate increased with the increase of τ_d^I . (E) The average CV of ISIs and the ratio between mean firing rate and peak frequency of network oscillation. (F) The average FF of individual neurons. (G) The FF of the network population spiking counts. (H) The FF of the population spiking counts in the field model. Time windows for measuring FFs are given in the figure legends. Averages are taken across the excitatory population for the measurements in (C-H). The external input is set as $Q_o = 5 \text{ Hz}$ in (B-H).

Scale-free neuronal avalanches near the critical transition point

For our mean-field theory of balanced networks, the Hopf bifurcation predicts that a global oscillation emerges in the field equations with oscillation amplitude growing continuously from zero. This picture is similar to a second-order phase transition in statistical physics when oscillation amplitude is taken as the order parameter. Thus, we measure the spiking avalanches (see *Materials and Methods* for further details) to examine whether this kind of criticality can result in scale-invariant spiking behaviour, i.e. critical avalanches, as observed in experiments [8–10]. Fig. 3B illustrates the time course of an avalanche.

To more clearly compare the feature of avalanche dynamics, raster plots of the spiking time of excitatory neurons in three typical cases are shown in Fig. 3A. These plots illustrate the asynchronous state (upper panel), the onset of synchrony and oscillation (middle panel) and the fully developed collective oscillation (lower panel). Power spectrum density analysis of network firing rate is shown in Fig. 3D. The asynchronous state appears without collective oscillation (frequency peak) and the avalanche size and duration distributions are exponential-like, as shown by the blue curves in Fig. 3E and F. It is thus subcritical. The onset of synchrony is usually accompanied by a frequency peak of fast oscillation situated within the gamma bands, which is thought to have functional importance in various cognitive processes [7]. This fast oscillation is temporally organised as scale-invariant avalanches, with power-law-like size and duration distributions, as shown by the green curves in Fig. 3E and F and it is thus a critical state. It can be seen from Fig. 2C that the average pairwise correlation is still low in the critical state, since the avalanches at this stage are only randomly participated by a small portion of neurons (Fig. 2E), which reconciles the coexistence of weak pairwise correlation and strong clustered spiking patterns [17]. The collective oscillation state has more slow frequency peaks and the avalanche size and duration distributions have heavier tails (corresponding to the red curves in Fig. 3E and F) compared with the critical state, which are features of a supercritical state.

We examine the distance D between the avalanche size distribution and its fitted power-law distribution (see *Materials and Methods* for further details). Fig. 3D shows that the network was closest to criticality when poised near the Hopf bifurcation point predicted by the mean-field theory. The existence of power-law distribution is only partial evidence of criticality, as other mechanisms could generate power-law distribution [49]. We further examined the scaling relation [43] in the critical state (see *Materials and Methods* for further details). The estimated slopes in the avalanche size and the duration distributions define the critical exponents $P(S) \sim S^{-\tau}$ and $P(T) \sim T^{-\alpha}$. A third exponent is defined as $\langle S \rangle(T) \sim T^{1/\sigma\upsilon z}$, where $\langle S \rangle(T)$ is the average size of avalanches with the same duration T . The third scaling feature can be found in both the subcritical and critical cases (Fig. 3G), in accordance with previous experimental findings [11]. We find that the scaling relation [43]

$$\frac{\alpha-1}{\tau-1} = \frac{1}{\sigma\upsilon z} \quad (6)$$

approximately holds at the critical state. The exact value of critical exponents may depend on the details of the system. As can be seen in Fig. 3H, different exponents keeping the scaling relation Eq. (6) can be found by varying the input strength Q_o . The critical exponents predicted by the model

are also close to the ranges ($\alpha_{\text{exp}}, \tau_{\text{exp}}$ vary between $1.3 \sim 2.5$ while $\frac{1}{\sigma\upsilon z_{\text{exp}}} \approx 1.28$ universally holds,

with the scaling relation Eq. (6) maintained) measured *in vivo* in the primary visual cortexes (V1) of various animals [18] across a wide range of neural activity states. Furthermore, in the model we find an approximate linear relationship between exponents τ and α whereby $\alpha = 1.21\tau - 0.154$, as shown in Fig. 3H, inner panel. Note that such a linear relationship between exponents τ and α is also found in V1 data [18] with $\frac{1}{\sigma\upsilon z_{\text{exp}}} \approx 1.28$ preserved, such that $\frac{\alpha-1}{\tau-1} = 1.28 \Leftrightarrow \alpha = 1.28\tau - 0.28$.

Here we show that this linear relationship can be maintained with slightly different values of $\frac{1}{\sigma\upsilon z}$.

We speculate that the relationship may depend on the properties of the underlying system at criticality (see the experimental data analysis below). The scaling relation expressed by Eq. (6)

provides additional evidence that the avalanches in the microscopic network occurring near the bifurcation point of the mean field model possess the properties of criticality.

Note that an avalanche can be understood as a temporal propagation of spiking activity in a network. On the macroscopic scale, this corresponds to a noise-induced excursion of the population firing rate. As our measurement of avalanches in the network by individual spiking times requires a fine time scale, and the information in this fine scale is averaged out in the field model, information describing small avalanches vanishes in the field model, which only predicts the global firing rate dynamics. Although it is still difficult to directly link the microscopic avalanches dynamics to the macroscopic firing rate dynamics, we show that scale-free behaviour near a synchronous transition point could be understood as a general feature of dynamic systems near a bifurcation point when subjected to demographic noise $dx/dt \sim \sqrt{x}\xi(t)$ [50] (see *Materials and Methods* for further details).

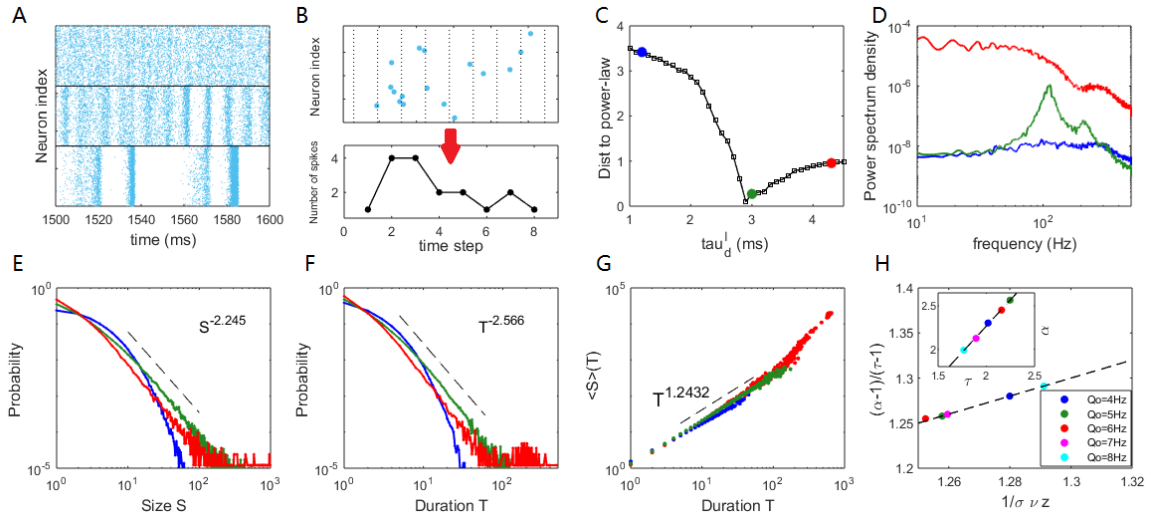


Fig. 3. Critical dynamics near the onset of collective oscillation. (A) The raster plots of the spiking time of the excitatory neurons at $\tau_d^l = 1.2 \text{ ms}$ (upper panel), $\tau_d^l = 3 \text{ ms}$ (middle panel) and $\tau_d^l = 4.3 \text{ ms}$ (lower panel). (B) An example of the time course of an avalanche. (C) The distance between the avalanche size distribution and its best-fitting power-law distribution. (D) The power spectrum density of the network excitatory firing rate. (E) The probability density distribution of the avalanche size. (F) The probability density distribution of the avalanche duration. (G) The mean avalanche size with respect to a given avalanche duration. For (D-G), the blue, green and red curves correspond to the cases of $\tau_d^l = 1.2, 3, 4.3 \text{ ms}$, respectively. (H) Scaling relation Eq. (6) approximately holds for critical states with different input strengths Q_o , where the dashed line represents Eq. (6) exactly holding. The inset shows an approximate linear relationship between exponents τ and α . Here, $\tau_d^l = 3.2 \text{ ms}$ is used for $Q_o = 4 \text{ Hz}$ and $\tau_d^l = 3 \text{ ms}$ is used for $Q_o = 5 \sim 8 \text{ Hz}$.

Validation of the theory in experimental data

To validate that irregular neuron spiking and collective critical avalanches coexist, we use public experimental data measuring the *in vitro* neuronal spiking activity of mouse somatosensory cortex cultures [44] (25 data sets in total). We measure the CV of ISIs and the avalanches during the up-states (see *Materials and Methods* for further details). In total, nine of the 25 data sets exhibit size and duration distributions that correspond to power-laws according to our standards (see *Materials and Methods* for further details). Among them, seven sets contain critical exponents that approximately satisfy the scaling relation Eq. (6) with errors < 0.1 . The statistical results of these seven data sets are shown in Fig. 4. These estimated critical exponents α , τ and $\frac{1}{\sigma \nu z}$ are also close

to the ranges found in our model. The boxplots of the distribution of CV of ISI across neurons in each set are shown in Fig. 4A. Typical values of CV of neuron ISI are around 1~1.5, a range similar to the model prediction, indicating irregular spiking. Fig. 4C to E illustrates the avalanche size and duration statistics of Set 1. Power-law distribution of avalanche size and duration can be observed. For surrogated data, where the inter-spike intervals of neurons were randomly shuffled, power-law distributions cannot be maintained, indicating that the critical properties are intrinsic in the data. As shown in Fig. 4B, the scaling relationship between critical exponents (i.e. Eq. (6)) approximately holds for these data sets. For these critical data sets, we also find a linear relationship between exponents τ and α (as seen in the inner panel of Fig. 4B) whereby $\alpha = 1.36\tau - 0.37$, while the slope is slightly different from the value in our model (inner panel, Fig. 3H). These results, obtained from experimental data, confirm the model prediction that irregular neuron spiking can collectively organise as scale-invariant critical avalanches.

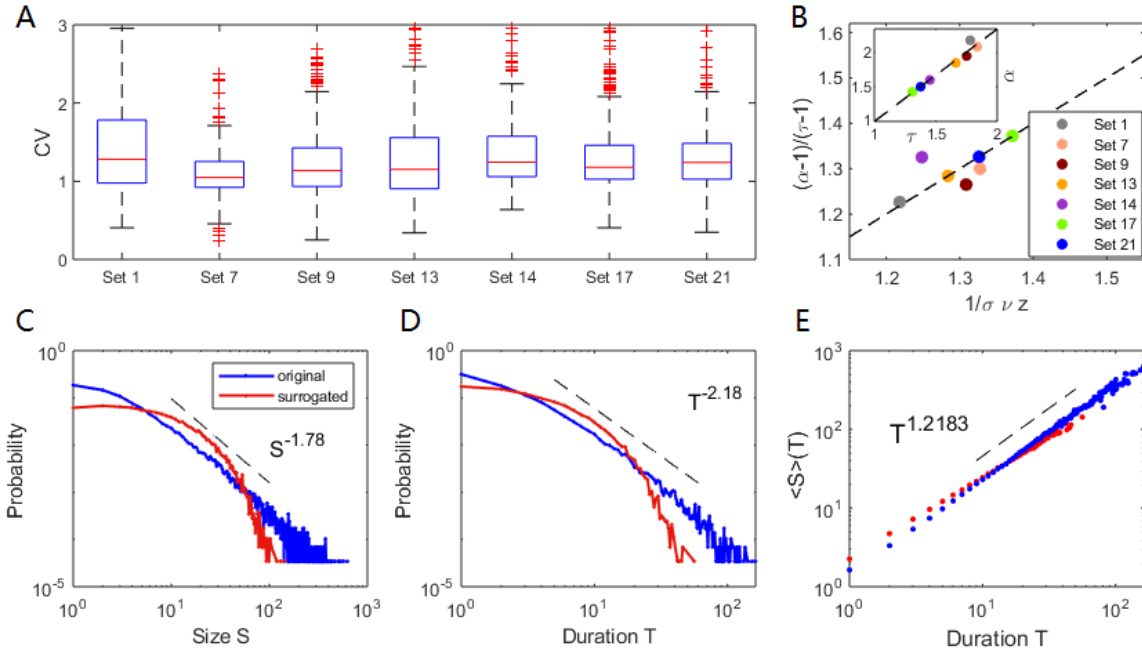


Fig. 4. Coexistence of irregular spiking and critical avalanches in experimental data sets. (A) Boxplots of the CV distribution across neurons in different data sets. (B) Scaling relations between

critical exponents of different data sets, similar to Fig. 3H. (C-E): critical avalanche properties of data Set 1. (C) Probability density distribution of the avalanche size. (D) Probability density distribution of the avalanche duration. (E) Mean avalanche size with respect to the given avalanche duration. The power-law distributions of size and duration are destroyed by surrogated data with shuffled ISI (denoted by red curves).

Discussion

In summary, we have shown that E-I balanced IF networks with synaptic filtering kinetics can reconcile the coexistence of irregular spiking and collective critical avalanches near a synchronous transition point. The mechanism is unveiled by the macroscopic field equations derived by a novel mean-field theory which effectively capture the network dynamics and the phenomenon is verified by the spontaneous spiking activities recorded *in vitro* in mouse somatosensory cortex cultures.

The E-I balanced state

Traditionally, E-I balance [48] has been deemed to be the origin of neuron spiking irregularity. Classical mean-field theory [22–24] predicts that irregular spiking is an asynchronous state with low spiking time correlation. However, input synchrony [51] has also been shown to contribute to the property of irregular spiking. This varied understanding raised the question of whether the E-I balance theory could be extended to include the property of synchrony. By incorporating synaptic kinetics, we have shown that collective network oscillation can emerge due to looser balance where individual neurons continue to spike irregularly. Thus, individual irregular spiking is compatible with collective network oscillation, i.e. synchronous spiking or synchronous inputs. Our theory shows that the balanced state can be a stable fixed point or a stable limit cycle on the macroscopic scale. The former induced by strict balance corresponds to the asynchronous state in accordance with the traditional theory, while the latter induced by loose balance corresponds to collective network oscillation, with critical dynamics during the transition between them. It thus answers the long-standing question of how neuronal spiking can be both temporally irregular and substantially correlated within the E-I balance framework. The critical dynamics where neurons are partially synchronous also provides an explanation of how weak pairwise correlation can induce abundant collective behaviour [17].

Possible origin of crackling noise in neural systems

The criticality of neural systems has been long debated. Experimental and theoretical studies [8,36,41,42] have suggested that critical avalanches exist in the E-I balanced state, while most models use unrealistic neural dynamics (such as spreading processes on networks) and the definition of E-I balance is usually ambiguous. Our theory with realistic synaptic dynamics shows that network dynamics can be either asynchronous or synchronous in the E-I balanced state and that critical avalanches exist near the transition point between these states. This discovery offers a more biologically plausible explanation of the origin of scale-free dynamics in neural systems, i.e. the dynamics are caused by a potential phase transition indicated by a Hopf bifurcation on the macroscopic scale of an E-I balanced neuronal network with biologically plausible synaptic kinetics. Our theory is thus consistent with the understanding that criticality occurs at the edge of a synchronous transition [36,37] with intermediate levels of spiking variability [18], and that critical avalanches can temporally organise as collective oscillations [9]. Significantly, in our model, the synaptic transmission is not instantaneous due to the filtering effect, which renders difficulty in the

distinction of the spatially causal relation [39] between successive spiking. The time binning avalanches we measure here are temporally causal (as in experimental measurements) but not necessarily spatially causal in the network. Thus, our estimated critical exponents do not agree with the spatially causal avalanches produced by critical branching processes [52] (i.e. directed percolation (DP) class), which predicts $\tau = 1.5$, $\alpha = 2$, $\frac{1}{\sigma \nu z} = 2$. Indeed, critical exponents different from the DP class have been found in previously reported experiments [18,53]. Our own analysis of the experimental data (Fig. 4) also confirmed the variation of the exponents while maintaining the scaling relationship Eq. (6). We further find that this variation can allow a linear relationship between exponents α and τ as in as other experimental data [18]. This linear relationship may depend on detailed properties of the underlying circuit and its dynamic origin remains to be further explored. Unlike our study of dynamical criticality here, another branch of study of neural criticality uses concepts in thermodynamics [54,55] (e.g. define criticality when a pre-defined specific heat estimated from neural activities diverges). It remains to be further studied whether such statistical criticality also emerges near the dynamical critical point in our theory.

A macroscopic description of IF neuronal networks

In traditional theory, the firing rate of an IF neuron can be estimated using statistics relating to the first-passage process of membrane potential with diffusion approximation [56]. Under the assumption of inputs with Gaussian white noise (without auto-correlation), the firing rate statistics can be derived from the first-passage time theory of the Ornstein-Uhlenbeck (OU) process [57]. However, the effect of synaptic filtering will induce memory effects so that the input noise is no longer white, which prevents a complete analytic treatment of the system (for fast decay synapses, the firing rate has been derived asymptotically through a singular perturbation method) [58]. Crucially, the f-I curve, which expresses the relationship between input current and output rate, derived from the first-passage time theory has a non- elementary functional form, meaning that a simplified form of the f-I curve has to be assumed to achieve analytical treatments. Self-consistent relation of steady-state firing rate of a network [59,60] can be derived by a presumed f-I curve.

A more challenging but also more useful issue that has attracted much recent attention is to find macroscopic transient dynamic descriptions of the neuronal networks. Schaffer et al. [61] derived the complex firing rate equations of IF networks through the eigenfunction expansion of the Fokker-Planck equation under diffusion approximation. Deriving rate equations of adaptive nonlinear IF networks has also been studied [62] under some effective approximation of the Fokker-Planck equation. Montbrió et al. [63] derived the rate equations for quadratic IF networks using the Lorentzian ansatz. This approach has been generalised to including gap junctions [64] and synaptic filtering kinetics [65]. Schwalger et al [66] developed a method to derive the stochastic rate equations of adaptive IF networks based on mean-field approximation of the renewal equation. In general, no universal method has been described to derive the macroscopic rate dynamics of IF networks. Most proposed theories failed to capture the synchronous transitions induced by the synaptic filtering effect studied in our model. Our theory contains a simple yet novel scheme that derives the dynamic equations governing the first-order statistics of the neural network. The key feature of our framework (detailed derivations are presented in *Materials and Methods*) is that the mean-field equations of the macroscopic dynamical variables can be closed by the voltage-dependent mean firing rate (i.e. Eq. (3)), which essentially captures the sub and supra threshold microscopic dynamics of a spiking network. The theory successfully explains the dynamic origin of the collective oscillation induced by prolonged inhibitory synaptic decay times in an E-I balanced network. Despite these successes, the theory cannot accurately compute exact firing rate

values because it neglects several factors that affect this rate, including higher order statistics, noise correlation and refractory time. Nonetheless, the theory provides a simple yet useful method to analyse dynamic features related to the network firing rate, such as synchrony, criticality and response.

Outlook

Thus, it is straightforward that the mean-field analysis introduced here can be used in the study of neural dynamics across a diverse range of topics. It can be easily generalized to include other factors by assuming different macroscopic variables in the field model. Possible extensions of the analysis include studying the effects of multiple neuronal populations and synaptic receptor types, cluster or spatially extended network connections, adaptive behaviours such as short-term plasticity, etc. Thus, our work allows further exploration of the physical mechanism that determines the role of synaptic kinetics in working memory retrieval [67], self-organised critical phenomena [68,69] and spatially causal avalanches or waves [30–32] arising from competition between Hopf and Turing instability [70]. As a theory that links microscopic neuronal spiking and macroscopic collective activity that are consistent in several aspects with real neural dynamics with regard to E-I balance and neural criticality, our theory also establish a base to model large-scale brain connectomes [71,72]. The potential applications of our theory listed here will receive the further exploration they deserve in due course.

Materials and Methods

Spiking neuronal network

We study a leaky IF spiking neuronal circuit. Neurons are coupled by a random network with density p and size $N = N_E + N_I$, which consists of N_E excitatory (E) neurons and N_I inhibitory (I) neurons. Thus, each neuron in the network has on average $n_E = pN_E$ E neighbours and $n_I = pN_I$ I neighbours. Each neuron also receives n_o excitatory inputs modelled by independent Poisson processes with frequency Q_o , mimicking external inputs for the circuit under consideration. We set $p = 0.2$, $N_E : N_I = 4 : 1$, $n_o = n_E$ and the network size is $N = 10^4$, unless otherwise specified. The sub-threshold membrane potential of neuron i at time t , denoted as $V_i(t)$, is governed by Eq. (1). The first term of Eq. (1) describes the leaky current $f_\alpha(V_i) = (V_{rest}^\alpha - V_i) / \tau_\alpha$, which has the effect to drive the membrane potential back to the leaky potentials, which are set to be $V_{rest}^E = V_{rest}^I = -70 \text{ mV}$. The membrane time constants are set as $\tau_E = 20 \text{ ms}$, $\tau_I = 10 \text{ ms}$ for E and I neurons, respectively. The second to fourth terms of Eq. (1) are the external, excitatory recurrent and inhibitory recurrent currents, respectively. Input currents are the summations of the filtered pulse trains. The synaptic filter is modelled as a bi-exponential function, i.e. Eq. (2). In Eq. (2), we set the synaptic rise time $\tau_r = 0.5 \text{ ms}$ for both E and I neurons, while the synaptic decay times τ_d^I, τ_d^E depend on the type of presynaptic neuron. We set $\tau_d^E = 2 \text{ ms}$ and let τ_d^I change from $1 \sim 4.5 \text{ ms}$ to study the effect of different E and I synaptic filtering time scales. The integration dynamics is as follows. When the membrane potential reaches the threshold $V_{th} = -50 \text{ mV}$, a spike is emitted and the membrane potential is reset to $V_{reset} = -60 \text{ mV}$. Then, synaptic integration is halted for 2 ms for E neurons and

1 ms for I neurons, modelling the refractory periods in real neurons. Synaptic weights are set as $J_{EO} = 45 \text{ mV}$, $J_{IO} = 72 \text{ mV}$, $J_{EE} = 36 \text{ mV}$, $J_{IE} = 72 \text{ mV}$, $J_{EI} = -81 \text{ mV}$ and $J_{II} = -144 \text{ mV}$, which will satisfy the balanced condition. Network dynamics are simulated by a modified second-order Runge-Kutta scheme [73] with a time step of $dt = 0.05 \text{ ms}$. For each parameter, the network is simulated for 16 s with the first 1 s discarded to avoid a transient effect. The statistical indexes are then computed by averaging the results of 15 trials with randomly distributed initial membrane potentials. The dynamics we considered here are current based. The case of conductance-based dynamics where the input of a neuron depends on its membrane potential is further studied in *Appendix I. Model Extensions*.

Mean-field theory of network dynamics

Derivation of the macroscopic field equations. We will develop a mean-field theory to approximate the average dynamics of the network by noting the fact that 1) the network topology is homogeneous and 2) the number of neuron N is large. The following mean-field derivation holds for large enough N and the network size is explicitly included in the field model equations (see Eqs. (17, 18) below).

We denote the average membrane potential of the network as $V_\alpha = \langle V_i \rangle_{i \in \alpha}$, $\alpha = \{E, I\}$. The goal is to derive a set of self-consistent field equations governing the temporal dynamics of V_α .

First, by noting that the convolution $F^\alpha * s_j(t - \tau_l^\alpha)$ obeys the equation

$$(\tau_d^\alpha \frac{d}{dt} + 1)(\tau_r \frac{d}{dt} + 1)[F^\alpha * s_j(t - \tau_l^\alpha)] = \sum_n \delta(t - t_j^n - \tau_l^\alpha), \quad (7)$$

then we have

$$(\tau_d^\alpha \frac{d}{dt} + 1)(\tau_r \frac{d}{dt} + 1) \left\langle \sum_{j \in \partial_l^\alpha} F^\alpha * s_j(t - \tau_l^\alpha) \right\rangle_{i \in E, I} = \left\langle \sum_{j \in \partial_l^\alpha} \sum_n \delta(t - t_j^n - \tau_l^\alpha) \right\rangle_{i \in E, I}. \quad (8)$$

Under mean-field approximation, each neuron is the same in terms of their neighbors, so that

$$\left\langle \sum_{j \in \partial_l^\alpha} \sum_n \delta(t - t_j^n - \tau_l^\alpha) \right\rangle_{i \in E, I} \approx n_\alpha Q_\alpha(t - \tau_l^\alpha), \quad (9)$$

where n_α is the average number of α neighbors of a neuron in the network and $Q_\alpha(t)$ is the mean firing rate of α type neurons, defined as

$$Q_\alpha(t) = \lim_{\Delta t \rightarrow 0} \frac{1}{\Delta t} \int_t^{t+\Delta t} \left\langle \sum_n \delta(s - t_j^n) \right\rangle_{j \in \alpha} ds. \quad (10)$$

In the standard definition of firing rate [74] of a neuron, the average in Eq. (10) is taken over different simulation trials. Since ergodicity and the network homogeneity, neurons within a population should have the same firing rate and it can be computed through Eq. (10) (i.e. population averages can be thought as sample averages) when the network is large enough. Formally, for

measuring the firing rate from data, the time interval Δt in Eq. (10) has to be finite. Here we choose $\Delta t = 1 \text{ ms}$ (shorter than the refractory period) so that a neuron can at most have one spike between t and $t + \Delta t$. Then, by the definition of δ function, $Q_\alpha(t)$ represents the proportion of α type neurons that spike between t and $t + \Delta t$ as well as the mean firing rate of α type neurons at time t with unit per ms.

In previous analysis framework of IF neurons through continuous stochastic process theory [56], the membrane potential V_i of neuron i cannot cross the spiking threshold (V_i is restricted to $(-\infty, V_{th})$ with V_{th} being an absorbing boundary). This is a theoretical artefact, contrary to the true neurophysiology. Furthermore, in numerical integration, the resetting is achieved by finding those neurons whose membrane potential increases over the spiking threshold in each numerical step [73]. This inspires us to naturally consider that a neuron j should have a spike at time t if $V_j(t) > V_{th}$. Formally, $V_j(t)$ can be considered as the membrane potential of neuron j at time t before the resetting rule in each numerical step. Thus,

$$Q_\alpha(t) = \langle H(V_j - V_{th}) \rangle_{j \in \alpha}, \quad (11)$$

where H is the Heaviside function $H(x) = \begin{cases} 1, & x \geq 0 \\ 0, & x < 0 \end{cases}$. Eq. (11) explicitly builds the link that the population firing rate is the proportion of the neurons whose membrane potential is above the spiking threshold. As a preliminary approximation, we assume $V_j(t)$ obey a Gaussian distribution $P_\alpha(V)$ with time-dependent mean $V_\alpha(t)$ and time-independent variance σ_α^2 . Then,

$$Q_\alpha(t) = \langle H(V_j - V_{th}) \rangle_{j \in \alpha} = \int_{V_{th}}^{\infty} P_\alpha(V) dV = \frac{1}{2} - \frac{1}{2} \text{erf}\left(\frac{V_{th} - V_\alpha}{\sqrt{2}\sigma_\alpha}\right), \quad (12)$$

where erf is the error function $\text{erf}(x) = \frac{2}{\sqrt{\pi}} \int_0^x e^{-t^2} dt$. Although there is no elementary expression for the error function, it can be approximated by elementary functions. For example, a good approximation that can keep the first and second moments is $\text{erf}(x) \approx \tanh(\frac{\pi x}{\sqrt{6}})$. Under this approximation, we have

$$Q_\alpha(t) = \frac{1}{2} - \frac{1}{2} \tanh\left(\frac{\pi}{\sqrt{6}} \frac{V_{th} - V_\alpha}{\sqrt{2}\sigma_\alpha}\right) = \frac{1}{1 + \exp\left(\frac{V_{th} - V_\alpha}{\sigma_\alpha} \frac{\pi}{\sqrt{3}}\right)}. \quad (13)$$

Here, the standard deviation of the voltage σ_α acts as an effective parameter to construct the voltage-dependent temporal firing rate and has to be estimated independently. For the current-based model we consider here, a simple estimation can be obtained from the diffusion approximation of the input noise. Note that each neuron receives n_o independent Poisson spike trains externally with rate Q_o . Thus, the input of each neuron has a variance $n_o Q_o$. If we do not consider its filtering effect since the fast decay time of excitatory synapse, by diffusion approximation we have

$$\frac{dV_i}{dt} \approx \text{const} - \frac{V_i}{\tau_\alpha} + J_{\alpha o} \sqrt{n_o Q_o} \xi_i(t), i \in \alpha \quad (14)$$

where $\xi_i(t)$ is a standard Gaussian white noise (GWN) with zero mean and unit variance. Note that in Eq. (14), we only assume that the noise is from external inputs since they are the direct independent noise source of the model. Thus, unlike many previous analytic theory [60] which assumes the input noise is contributed by external input, recurrent excitation and recurrent inhibition such that the variance of total input noise is $J_{\alpha o}^2 n_o Q_o + J_{\alpha E}^2 n_E Q_E + J_{\alpha I}^2 n_I Q_I$, we neglect the noise from recurrent inputs. Indeed, such an estimation overrates the noise strength since the recurrent inputs are not totally mutual independent especially when close to or beyond the onset of synchrony. The Langevin equation Eq. (14) predicts a Gaussian distribution for the voltage V_i with variance $J_{\alpha o}^2 n_o Q_o \tau_\alpha$. Thus, an estimation of σ_α is

$$\sigma_\alpha = \sqrt{J_{\alpha o}^2 n_o Q_o \tau_\alpha} \quad (15)$$

In general, σ_α is an effective parameter to represent the standard deviation of V_i when it is assumed to be Gaussian distributed. In any case, it can also be estimated numerically from the steady-state mean voltage V_α^{ss} and mean firing rate Q_α^{ss} and use Eq. (13) to get

$$\sigma_\alpha = \frac{V_{th} - V_\alpha^{ss}}{\ln((Q_\alpha^{ss})^{-1} - 1)} \cdot \frac{\pi}{\sqrt{3}} \quad (16)$$

For the results in the main text, the parameters σ_α are estimated by Eq. (15) whereas for the results on conductance-based models in *Appendix I. Model Extensions*, Eq. (16) is used. The sigmoid transfer function Eq. (13) is the intrinsic nonlinear property that induces oscillation transition in the field model. Note that neural field models of Wilson-Cowan type [75] would also contain a presumed sigmoid transfer function. Field models of this type can also qualitatively reproduce some dynamic features of E-I neuronal networks. Here we explicitly construct the sigmoid function from the microscopic spiking network. Thus, once σ_α are chosen as suitable values, our field equations can predict the dynamics of the E-I network quantitatively (see *Appendix II. Sensitivity of the critical points on the effective parameters* where we study the sensitivity of the oscillation transition with respect to the effective parameters σ_α).

Denote $\Phi_\alpha(t) = \left\langle \sum_{j \in \partial_i^\alpha} F^\alpha * s_j(t - \tau_i^\alpha) \right\rangle_{i \in E, I}$ as the averaged synaptic time course of α inputs

received by a neuron and from Eqs. (8, 9, 13) it will obey

$$(\tau_d^\alpha \frac{d}{dt} + 1)(\tau_r \frac{d}{dt} + 1)\Phi_\alpha(t) = n_\alpha / (1 + \exp(\frac{V_{th} - V_\alpha(t - \tau_i^\alpha)}{\sigma_\alpha} \frac{\pi}{\sqrt{3}})), \alpha = E, I \quad (17)$$

From the illustration of Eq. (14), we know that the external input $\sum_{j \in \partial_i^o} F^E * s_j(t - \tau_i^E)$ of each neuron can be approximated by $n_o Q_o + \sqrt{n_o Q_o} \xi_i(t)$ in the diffusion approximation. Since $\xi_i(t)$ are independent GWNs, $\langle \sqrt{n_o Q_o} \xi_i(t) \rangle_{i \in \alpha}$ can be equivalently approximated by $\sqrt{n_o Q_o / N_\alpha} \xi_\alpha(t)$, where

$\xi_\alpha(t)$ is another standard GWN. Thus, taking the average $\langle \cdot \rangle_\alpha$ of the original equation Eq. (1) and note that in the leaky IF model, f_α is linear, we arrive at

$$\frac{dV_\alpha}{dt} = f_\alpha(V_\alpha) + J_{\alpha o}(n_o Q_o + \sqrt{n_o Q_o / N_\alpha} \xi_\alpha(t)) + J_{\alpha E} \Phi_E + J_{\alpha I} \Phi_I, \alpha = E, I. \quad (18)$$

In the field equation Eq. (18), $\xi_E(t)$ and $\xi_I(t)$ are two independent GWNs. We find that this approximation is independent of the nature of noise in the spiking network model. In the network model Eq. (1), the nature of noise from external inputs is synaptic-filtered Poisson shot noise. We further examine the case where external inputs in Eq. (1) are with GWNs and the case of constant external input (i.e. no noise) and find that in such cases Eq. (18) can still well approximate the macroscopic dynamics of the network (for constant external input the network dynamics is not stochastic, but the spiking activity still appears irregular due to the chaotic nature of the network [22,23]). Generally speaking, the mean-field theory only holds when the system size is infinity. The incorporation of noise into the field model can smooth out the systematic errors, compensate the finite size effect and make it closer to the true rate dynamics statistically. Thus, for numerical simulation of the field equations we will keep the noise terms in Eq. (18) whereas the deterministic counterpart would be used for stability analysis.

In summary, we have proposed a novel technique to derive a set of self-consistent field equations Eqs. (17, 18), that is, Eqs. (4, 5), to approximate the average dynamics of the original spiking network Eqs. (1, 2).

Analysis of the steady-state dynamics. The deterministic steady-state (fixed point) of the field model can be found from Eqs. (17, 18) by letting $d/dt = 0$ and assume $\xi_\alpha(t) = 0$, resulting in algebraic equations

$$f_\alpha(V_\alpha) + J_{\alpha o} n_o Q_o + J_{\alpha E} n_E Q_E + J_{\alpha I} n_I Q_I = 0, \alpha = \{E, I\}. \quad (19)$$

where Q_E, Q_I are given by Eq. (13). In our case, the synaptic strengths and external input rates are the major parameters determining the value of the fixed point, while synaptic decay time would affect its stability. This is because the value of steady-state does not depend on τ_d^α, τ_r , which can also be seen from Eq. (2) that the synaptic filter is normalized ($\int_0^\infty F^\alpha * \delta(t) dt = 1$ independent of τ_d^α, τ_r) so that synaptic rise and decay times would not affect the time-averaged firing rate. Thus, the scheme here cannot capture the nontrivial effect of synaptic filtering on affecting the firing rate (e.g. see the formula given by Fourcaud and Brunel [58]). Note that in general settings of balanced networks with dense and strong coupling [24], the quantities n_o, n_E, n_I are of order $O(N)$ but the synaptic weights are of order $O(N^{-1/2})$. When N is large enough, the first term in Eq. (19) can be neglected and it reduces to

$$J_{\alpha o} n_o Q_o + J_{\alpha E} n_E Q_E + J_{\alpha I} n_I Q_I = 0, \alpha = \{E, I\}, \quad (20)$$

which is a set of linear equations to solve the steady firing rate Q_E, Q_I . To guarantee a unique positive solution in this case, the sequence $\{\frac{J_{EO}}{J_{IO}}, \frac{J_{EI}}{J_{II}}, \frac{J_{EE}}{J_{IE}}\}$ should be in ascending or descending

order, which is the so-called balanced condition in the traditional theory [22–24]. Thus, the theory here is a generalization of the traditional theory of balanced network.

In the traditional theory of asynchronous dynamics, the E-I balanced state can be considered as the existence of a stable fixed point of Eqs. (17, 18). Now we can consider how the stability of this fixed point can be changed with the aid of this dynamic form. For the case without synaptic delay (i.e. $\tau_l^E = \tau_l^I = 0$), the field equations are ordinary differential equations. By taking $X = (V_E, V_I, \Phi_E, d\Phi_E / dt, \Phi_I, d\Phi_I / dt)$, the field model Eqs. (17, 18) can be written in the first-order form $\frac{dX}{dt} = F(X)$ without considering the noise. The Jacobian matrix at the steady state is

$$J = \begin{pmatrix} -1/\tau_E & 0 & J_{EE} & 0 & J_{EI} & 0 \\ 0 & -1/\tau_I & J_{IE} & 0 & J_{II} & 0 \\ 0 & 0 & 0 & 1 & 0 & 0 \\ \frac{n_E Q'_E(V_E)}{\tau_d^E \tau_r} & 0 & -\frac{1}{\tau_d^E \tau_r} & -\frac{1}{\tau_d^E} - \frac{1}{\tau_r} & 0 & 0 \\ 0 & 0 & 0 & 0 & 0 & 1 \\ 0 & \frac{n_I Q'_I(V_I)}{\tau_d^I \tau_r} & 0 & 0 & -\frac{1}{\tau_d^I \tau_r} & -\frac{1}{\tau_d^I} - \frac{1}{\tau_r} \end{pmatrix} \quad (21)$$

with $Q'_\alpha(V_\alpha) = \frac{\pi \exp[(V_{th} - V_\alpha)\pi / (\sqrt{3}\sigma_\alpha)]}{\sqrt{3}\sigma_\alpha (1 + \exp[(V_{th} - V_\alpha)\pi / (\sqrt{3}\sigma_\alpha)])^2}$ estimated at the steady-state value of V_α given by Eq. (19). The eigenvalues of J can determine the stability of the steady state. Note that many models use single exponential function as the synaptic filter, i.e. $\tau_r = 0$, and in this case the dynamic form becomes 4-dimensional with $X = (V_E, V_I, \Phi_E, \Phi_I)$. For models without considering synaptic filtering effect (that is, the case of instantaneous synapse where $\tau_r = \tau_d^\alpha = 0$), the dynamic form becomes 2-dimensional, which can be considered as the dynamic form of traditional theory without synaptic kinetics. In these cases, the stability analysis can be performed in a similar way. In the presence of synaptic transmission delay, the field equations would become delay differential equations. In this case, stability analysis would in general become more difficult.

Critical properties near the bifurcation point. Although it is still difficult to directly link the microscopic avalanches dynamics to the macroscopic firing rate dynamics, the properties of burst activities (avalanche) in the macroscopic scale can shed light on the origin of power-law scaling in the microscopic network.

To consider the avalanche in the macroscopic scale, one should inspect the fluctuation behavior of a macroscopic signal $x(t)$ of the network, such as the mean firing rate, etc. An avalanche is a process that starts growing at $x(0) = x_{th} + \varepsilon$ ($\varepsilon \rightarrow 0^+$) and at the first time it goes back to $x(T) = x_{th}$ at time $t = T$. Here, x_{th} is a threshold above which the avalanche is defined. Such an approach is often used to measure neural avalanche in macroscopic signal such as magnetoencephalography (MEG) [76]. The quantity T turns out to be the first-passage time (FPT) (back to x_{th}) of this process

and it defines the duration of an avalanche. The area $S = \int_0^T x(t)dt$ in this process defines the size of the avalanche.

The scale-free behavior at the synchronous transition point can be understood as the general feature of dynamical systems near a bifurcation point when subjected to demographic noise $dx/dt \sim \sqrt{x}\xi(t)$ [50]. This is because the E-I network here is subjected to Poisson-like noise and the overall fluctuation of population activity density scales with its square root as given by the central limit theorem [37,77]. Noise-driven random walker theory predicts that power-law distribution of the avalanche is a general feature of a dynamical system subjected to such kind of noise when near the Hopf bifurcation (actually, general bifurcations) point. Specifically, although the dynamic form of this macroscopic signal may not be explicit in the field equations, we can heuristically consider a situation that $X(t) = x - x_h$ obeys an intrinsic dynamic as the normal form of the amplitude dynamics of Hopf bifurcation but driven by noisy force. The Langevin equation it obeys is

$$\frac{dX}{dt} = aX - X^3 + \eta(X, t). \quad (22)$$

The first part of Eq. (22) is the normal form of the oscillation amplitude dynamics of a supercritical Hopf bifurcation [78] and periodic motion arises when a increases across the bifurcation point $a=0$. The second part $\eta(X, t)$ is the noisy driving force, where GWN is assumed for analytical treatment and the fluctuation scales with square root of the activity. Thus, it has the form $\eta(X, t) = h + \sqrt{X}\xi(t)$, where h is the mean bias, including the effect from recurrent excitatory, recurrent inhibitory and external inputs. $\xi(t)$ is a standard GWN. The fact is that avalanche dynamics given by the first-passage process of Eq. (22) can be mapped to the case of random walks in logarithmic potential [50] by a scaling analysis (details in Ref [50]). Under this approach, the FPT distribution of the avalanche process can be solved by absorbing boundary approach in an analytical way, resulting in

$$P(T = t) = \frac{(\sqrt{2}\varepsilon)^{1-4h}}{\Gamma(1/2-h)} t^{\frac{4h-3}{2}} \exp\left(-\frac{2\varepsilon^2}{t}\right). \quad (23)$$

This explains the power-law distribution relation $P(T) \sim T^{-\alpha}$ with $\alpha = \frac{3}{2} - 2h$ and other exponents can be obtained by scaling argument [50], although the relation between the avalanche critical exponents in the macroscopic scale and the microscopic scale needs further exploration. In all, the scale-free avalanche dynamics in the microscopic spiking network at the critical state may be understood as the scaling features of the first-passage dynamics near the Hopf bifurcation point in the macroscopic field model.

Statistical analysis of model and experiment data

Spike count series. For statistically analysing neural dynamics, the neuron spike train series have to be constructed from the model simulation data or the experimental data as follows. The time axis is first divided into consecutive time windows with sizes Δt ms. The number of spikes of neuron i are then counted in each window to obtain a discrete sequence $N_i(t)$, which is designated as the

spike count series of neuron i with time windows Δt . Alternatively, the number of spikes of the whole neuron population can be counted in each window. This constructs the population spike count series $N_\alpha(t)$ for the E and I populations, respectively. Furthermore, $q_\alpha(t) = \frac{N_\alpha(t)}{n_\alpha \Delta t}$ is the

population averaged firing rate series and the power spectrum of the population firing rate series can indicate the collective oscillation properties. For computing certain quantities, such as the correlation between neurons, the spike count series is filtered by a square kernel

$$K_T(t) = \begin{cases} 1/T, & t \in [-T, 0] \\ 0, & \text{other} \end{cases} \quad \text{with length } T \text{ and the ensuing filtered spike train is defined as}$$

$$n_i(t) = K_T * N_i = \frac{1}{T} \sum_{s=0}^{T-1} N_i(t-s).$$

Quantifying spiking irregularity and firing rate variability. The spiking time irregularity of a neuron can be quantified using the CV (coefficient of variance), which is defined as the standard deviation of the neuron ISIs (inter-spike intervals) over its mean. Totally regular activities have CV values of 0, while Poisson processes have CV values of 1. A higher CV value indicates larger irregularity. The firing rate variability on the individual neuron level and the population level can be measured by the relevant Fano Factor (FF). The FF of neuron i is defined as $FF_i = \text{var}(N_i(t)) / \langle N_i(t) \rangle$. The average and the variance here are taken across the spike count series.

Similarly, population FF is defined as $FF_\alpha = \text{var}(N_\alpha(t)) / \langle N_\alpha(t) \rangle$. The population FF can also be computed using the macroscopic field equations, as the field equations predicts the population firing rate, which can be transferred to population spike counts (by multiplying the number of neurons in the population). Note that FF depends on the time window size Δt to construct the spike count series.

Quantifying network synchrony. The synchrony of the network can be characterised from two aspects: the cross-correlation of spiking times and the coherence of the membrane potential [79]. The former quantifies the coherence of threshold events whereas the later quantifies the coherence of the subthreshold dynamics.

We employ the commonly used Pearson correlation coefficient (PCC) to quantify the synchrony of the spiking time. The spike count series of neuron i is first constructed with time window $\Delta t = 1\text{ms}$ and then filtered by a square kernel with length $T = 50\text{ms}$. Note that no more than one spike within 1 ms occurs for an individual neuron. The PCC between neuron i and j is defined as

$$c_{ij} = \frac{\text{cov}(n_i, n_j)}{\sqrt{\text{Var}(n_i)\text{Var}(n_j)}}. \quad \text{The details such as filtering in calculating PCC would affect its exact value}$$

[80], but not the qualitative change. The index $\langle c_{ij} \rangle_{i,j \in E}$, PCC averaged over all excitatory neuron pairs, is used to quantify the network synchrony degree of threshold events.

The voltage series of each neuron is constructed for each millisecond that $V_i(k) = V_i(t)|_{t=k\text{ms}}$. Voltage coherence is defined as $\rho = \sqrt{\sigma_m^2 / \langle \sigma_i^2 \rangle_{i \in \alpha}}$, where $\sigma_m^2 = \langle V_m^2 \rangle_t - \langle V_m \rangle_t^2$ is the variance of the

mean voltage $V_m = \langle V_i \rangle_{i \in \alpha}$ and $\sigma_i^2 = \langle V_i^2 \rangle_t - \langle V_i \rangle_t^2$ is the variance of the voltage of neuron i . The voltage coherence of the excitatory population is used to quantify the coherence of the subthreshold dynamics.

We further use the CV of the excitatory population firing rate series constructed with $\Delta t = 1ms$ to quantify temporal firing rate variability at short timescales, which is another way of indicating the network synchrony, as stronger synchrony indicates larger population firing rate variability at short timescales.

Neuronal avalanche analysis. We measure the neuronal avalanches of the excitatory neuron population from its population spike count series $N_E(t)$ constructed with window (bin) size Δt . An avalanche is defined as a sequence of consecutive non-empty bins, separated by empty bins (with no spiking inside). The size S of an avalanche is defined as the total number of spikes within the period and the duration T is defined as the number of time bins it contains. To compare different data sets in a unified standard, window size is chosen as the average ISI of the merged spiking train (constructed by merging the spike trains of all neurons). Thus, it depends on the mean firing rate of neurons in different data sets. This choice has been described as the ‘optimal’ window size to measure avalanches [8], as excessively small or large windows would lead to systematic bias. A further advantage of this choice is that the measured size and duration would approximately lie in the same scale ranges, allowing better comparison. Note that the definition of avalanche here is the time-binning (non-causal) avalanche, which corresponds to the case of experimental measurement [8,10], but is different from the causal avalanche [81] studied by many physical models rooted in critical branching processes.

Avalanche size obeying a power-law distribution is a typical sign of scale-invariance, which is a statistical property. We use a simple method to quantify how far the avalanche size distribution deviates from a power-law distribution. The avalanche size frequency distribution histogram $(S, P(S))$, is first obtained with 80 bins from minimum to maximum size. The least squares method is then used to find the best-fit-line in doubly logarithmic coordinates, such that $\sum_s [\lg P(S) - (b_0 + b_1 \lg S)]^2$ is minimised. After obtaining the best-fit coefficients (b_0, b_1) , the fitted frequency distribution values were estimated as $P_{fit}(S) = 10^{b_0 + b_1 \lg S}$. Finally, the normalised distance, defined as $D = \sum_s S |P(S) - P_{fit}(S)| / \sum_s S P(S)$, the average size difference per avalanche between the actual and fitting frequency distribution normalised by the mean avalanche size, is used to measure the distance to the best fitting power-law distribution. This distance acts as an index to indicate the degree of criticality for comparison.

The maximum likelihood estimation (MLE) method using the NCC toolbox [82] is used to estimate the critical exponents. The toolbox provides a doubly truncated algorithm based on the MLE to find the range that passed the truncation based KS statistics test [82]. This truncation scheme can avoid the noise (in the small avalanche size range) and finite size effect (in the large avalanche size range) interruption in estimating the critical exponents. We find the truncated range that can pass the KS-based test with a p value larger than 0.1 and boarder than one-third of the whole range on the logarithm scale. This means that the data can produce a KS-statistics value that is less than the values generated by at least 10% of the power-law models in the truncated range. The estimated slopes within the truncated ranges in the avalanche size and duration distributions

define the critical exponents $P(S) \sim S^{-\tau}$ and $P(T) \sim T^{-\alpha}$. A third exponent is defined as $\langle S \rangle(T) \sim T^{1/\sigma\nu z}$, where $\langle S \rangle(T)$ is the average size of avalanches with the same duration T . This exponent is fitted using a weighted least squares method [82] to those avalanches that fall into the truncated duration range for estimating α .

Experimental data analysis. We used the public experimental data measuring the neuronal spiking activity in mouse somatosensory cortex cultures *in vitro* [44]. A total of 25 data sets were used and the length of each record is one hour, with the exception of Set 19, which was 48 minutes long. The recordings were performed on organo-typical slice cultures after two to four weeks *in vitro*, without stimulation [83]. Spiking times were sorted with a PCA-based algorithm [84] to locate the signals recorded with a large and dense multi-electrode array of 512 electrodes.

Under *in vitro* conditions, spiking in the culture clearly shows up-down state transition. Active spiking periods (up-state) and silent periods (down-state) alternated slowly with a frequency of *circa* 0.1 Hz. Since spikes were too few in the down-states, we focus on analysing the up-state, which is more likely to represent normal neural activities. For each data set, the population firing rate series was first constructed with a time window of $\Delta t = 10ms$ and then filtered by a square kernel with length $T = 100ms$. Here, the up-state is defined as the time periods that the population firing rates are higher than 30% of the maximum rate of the given dataset and last longer than 1s. We measure the CV of ISIs and the avalanches in the up-states. The time bin for measuring the avalanche was the mean ISI, averaged through the up-state, of the merged spike train. To test critical properties, we first determine whether the size and duration distribution is close to a power-law and then estimate its critical exponents. As in our analysis of modelling data, the doubly truncated and statistical test algorithm from the NCC toolbox [82] is used. We accept the power-law distribution of a data set if the following two conditions can be jointly satisfied: 1) the truncated range has to be boarder than one-third of the whole range in the logarithm scale and; 2) the data in the truncated range can pass the KS-based test with p value larger than 0.1. Detailed results are shown in the table S1. For the cases deemed to be power-law distribution, the truncated ranges, estimated exponents and p values in the KS-based test are shown. For the data sets that have power-law avalanche distributions in both size and duration, we further compare the critical exponents $\frac{1}{\sigma\nu z}$ and the value $\frac{\alpha-1}{\tau-1}$ to see whether scaling relation Eq. (6) holds. To test whether power-law distribution is the intrinsic structure of the data, we also analyse the surrogated data constructed by randomly shuffling the ISIs of neurons in each up-state period. This random shuffling can destroy the intrinsic temporal correlation structures of the avalanches.

Appendix I. Model extensions

Extension to time-varying inputs

The field model Eqs. (17, 18) can be conveniently used to compute the transient firing rate dynamics of the network in response to the time-varying external input. For inhomogeneous Poisson external inputs with time-dependent firing rate $Q_o(t)$, the constant term Q_o in Eq. (18) can

just be modified to the time-dependent term $Q_o(t)$ and the field model can be simulated directly in this way. Note that a good estimation of the effective parameter σ_E, σ_I may depend on Q_o , as given by Eq. (15). However, we point out that if $Q_o(t)$ does not change very strongly, the parameters σ_E, σ_I can be kept constant throughout the change of $Q_o(t)$ once they have been estimated. To demonstrate this, we set a time-varying input

$$Q_o = \begin{cases} \lambda, & t \in [0, 200) \\ 4\lambda, & t \in [200, 400) \\ 2\lambda, & t \in [400, 500) \\ 2\lambda(1 + \sin[\frac{\pi}{100}(t - 500)]), & t \in [500, 800] \end{cases} \quad (24)$$

with $\lambda = 5Hz$ for each neuron as shown in Fig. S1A. Here, we do not consider the synaptic transmission delay and the synaptic decay times are set as $\tau_d^E = \tau_d^I = 4ms$, $\tau_r = 0$ where the network would be in asynchronous dynamics. Note that the external input $Q_o(t)$ contains constant part, discontinuous jumps and continuous changes. Simulations show that the firing rate changes accordingly respondent to the change of input, as can be seen from the raster plot in Fig. S1B. At the same time, we can simulate the field model Eqs. (17, 18) with the same time-varying input $Q_o(t)$ and constant parameters σ_E, σ_I estimated by Eq. (15) with $Q_o = \lambda$. As shown in Fig. S1C, the field model predicts the changing trend of the average firing rate of the network. It should be noted that this simple scheme ignores some complex nature of the firing rate response properties in the presence of synaptic filtering [85].

Extension to conductance-based models

The present mean-field theory can be directly generalized to conductance-based (COB) model where the postsynaptic inputs received by each neuron depend on the membrane potential of the neuron. Specifically, we further study a COB model with the dynamic equation Eq. (1) replaced by

$$\frac{dV_i}{dt} = f_\alpha(V_i) + (V_E^{rev} - V_i)(g_{\alpha O} \sum_{j \in \mathcal{O}_i^O} F^E * s_j(t - \tau_l^E) + g_{\alpha E} \sum_{j \in \mathcal{O}_i^E} F^E * s_j(t - \tau_l^E)) + (V_I^{rev} - V_i)g_{\alpha I} \sum_{j \in \mathcal{O}_i^I} F^I * s_j(t - \tau_l^I). \quad (25)$$

Here, the reversal potential for excitatory and inhibitory synaptic currents are $V_E^{rev} = 0mV$ and $V_I^{rev} = -70mV$ respectively. The synaptic strengths of conductance are set as $g_{EO} = 0.025, g_{IO} = 0.04$, $g_{EE} = 0.02, g_{IE} = 0.04$, $g_{EI} = 0.27, g_{II} = 0.48$. Other notations, parameters and settings are the same as the current-based (CUB) case. Similar to the CUB model, the COB model shows emergence of collective oscillation induced by slow inhibition. Such a critical transition can also be predicted by our mean-field theory as a Hopf bifurcation, while the derivation of the field equation is slightly different. In the CUB case, the field equation Eq. (18) can be obtained by taking the average $\langle \cdot \rangle_\alpha$ of the original equation Eq. (1) under mean-field assumption. In the COB case, we still can take the average $\langle \cdot \rangle_\alpha$ of the Eq. (25) under mean-field assumption, but have to proceed with the decoupling assumption that

$$\left\langle V_i (g_{\alpha E} \sum_{j \in \partial_i^E} F^E * s_j(t - \tau_l^E) + g_{\alpha I} \sum_{j \in \partial_i^I} F^I * s_j(t - \tau_l^I)) \right\rangle_{i \in \alpha} \approx \langle V_i \rangle_{i \in \alpha} \left\langle g_{\alpha E} \sum_{j \in \partial_i^E} F^E * s_j(t - \tau_l^E) + g_{\alpha I} \sum_{j \in \partial_i^I} F^I * s_j(t - \tau_l^I) \right\rangle_{i \in \alpha} \quad (26)$$

This is based on the fact that in an E-I balanced network where neurons spike irregularly, one expects that at any given time t , the correlation between the membrane potential and the recurrent E, I conductance input for different neurons is small. As such, we get the field equations

$$\frac{dV_\alpha}{dt} = f_\alpha(V_\alpha) + (V_E^{rev} - V_\alpha)(g_{\alpha o}(n_o Q_o + \sqrt{n_o Q_o / N_\alpha} \xi_\alpha(t)) + g_{\alpha E} \Phi_E) + (V_I^{rev} - V_\alpha)g_{\alpha I} \Phi_I, \alpha = E, I \quad (27)$$

to replace Eq. (18), where the quantity $\Phi_\alpha(t) = \left\langle \sum_{j \in \partial_i^\alpha} F^\alpha * s_j(t - \tau_l^\alpha) \right\rangle_{i \in E, I}$ still obeys Eq. (17). Thus, Eqs. (17, 27) constitute the field equations of the COB model Eq. (25).

In the CUB model, the effective parameters σ_E, σ_I can be estimated through Eq. (15). This estimation breaks down in the COB model since the multiplicative nature of the noise. Indeed, the COB input would lead membrane potential bias to a Gaussian distribution [86]. However, the sigmoid relation Eq. (13) can still be assumed and σ_E, σ_I can be estimated in a numerical way through Eq. (16).

A summarization and comparison between the field equations of CUB model Eq. (1) and COB model Eq. (25) is as follows.

$$\begin{aligned} \text{CUB: } \begin{cases} \frac{dV_\alpha}{dt} = f_\alpha(V_\alpha) + J_{\alpha o}(n_o Q_o + \sqrt{n_o Q_o / N_\alpha} \xi_\alpha(t)) + J_{\alpha E} \Phi_E + J_{\alpha I} \Phi_I \\ (\tau_d^\alpha \frac{d}{dt} + 1)(\tau_r \frac{d}{dt} + 1)\Phi_\alpha(t) = n_\alpha / (1 + \exp(\frac{V_{th} - V_\alpha(t - \tau_l^\alpha)}{\sigma_\alpha} \frac{\pi}{\sqrt{3}})) \\ \sigma_\alpha = \sqrt{J_{\alpha o}^2 n_o Q_o \tau_\alpha} \text{ or } \frac{V_{th} - V_\alpha^{ss}}{\ln((Q_\alpha^{ss})^{-1} - 1)} \cdot \frac{\pi}{\sqrt{3}} \end{cases}, \alpha = E, I \\ \\ \text{COB: } \begin{cases} \frac{dV_\alpha}{dt} = f_\alpha(V_\alpha) + (V_E^{rev} - V_\alpha)(g_{\alpha o}(n_o Q_o + \sqrt{n_o Q_o / N_\alpha} \xi_\alpha(t)) + g_{\alpha E} \Phi_E) + (V_I^{rev} - V_\alpha)g_{\alpha I} \Phi_I \\ (\tau_d^\alpha \frac{d}{dt} + 1)(\tau_r \frac{d}{dt} + 1)\Phi_\alpha(t) = n_\alpha / (1 + \exp(\frac{V_{th} - V_\alpha(t - \tau_l^\alpha)}{\sigma_\alpha} \frac{\pi}{\sqrt{3}})) \\ \sigma_\alpha = \frac{V_{th} - V_\alpha^{ss}}{\ln((Q_\alpha^{ss})^{-1} - 1)} \cdot \frac{\pi}{\sqrt{3}} \end{cases}, \alpha = E, I \end{aligned}$$

The calculation of the steady-state and its stability analysis at zero transmission delays can be performed in the same way as in CUB model. The qualitative results are similar to the CUB model. There is a critical value τ_d^{I*} such that when $\tau_d^I < \tau_d^{I*}$ the steady-state is a stable focus, corresponding to the asynchronous strict balance state of the network. For $\tau_d^I > \tau_d^{I*}$, the steady-state destabilizes through a supercritical Hopf bifurcation (Fig. S1D), corresponding to the onset of collective

oscillation in the network, as shown by the PCC in Fig. S1E. The spiking of individual neurons are still irregular, as can be seen from the high CV of ISIs in Fig. S1F. Furthermore, near the Hopf bifurcation point, the COB model exhibits critical properties in terms of avalanche dynamics similar to the results of CUB model (data not shown here). Overall, the quality of theoretical prediction in the COB case is worse than the CUB case. A complete analytical treatment of COB model is still challenging.

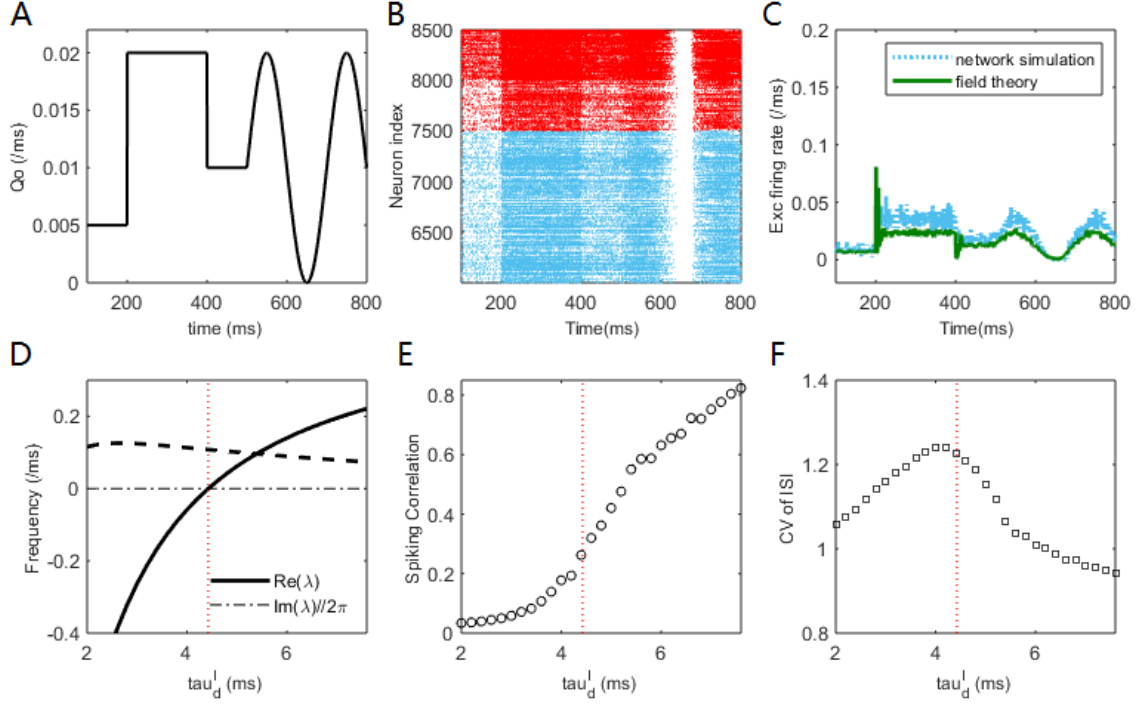


Fig. S1. Results of the generalized models. (A-C): Network dynamics in response to time-varying external input. (A) The time-dependent input function $Q_o(t)$ used in simulation. (B) Raster plot of the spiking time of neurons (only part of the $N=10000$ neurons are shown). The excitatory/inhibitory neurons are indicated in blue/red. (C) Comparison of the mean firing rate of excitatory population obtained by network simulation and field model simulation. (D-F): Mean-field theory prediction of the transition from asynchronous to synchronous state in COB model. (D) Field equations predict that a Hopf bifurcation occurs as the increase of inhibitory decay time τ_d^I at a critical value around $\tau_d^I \approx 4.4 \text{ ms}$. The real and imaginary part (divided by 2π) of the dominant eigenvalue are given by the solid and dashed lines, respectively. (E) The PCC index shows the emergence of network oscillation as the increase of τ_d^I across the bifurcation point. (F) The CV of ISI at different value of τ_d^I . The parameters in COB model are set as $\tau_r^E = \tau_r^I = 0 \text{ ms}$, $\tau_d^E = 2 \text{ ms}$, $\tau_r = 0 \text{ ms}$ and $Q_o = 5 \text{ Hz}$.

Appendix II. Sensitivity of the critical points on the effective parameters

The mean-field scheme to derive the field equations introduces two effective parameters σ_E, σ_I to construct the voltage-dependent firing rate relation Eq. (13) and they are the crucial quantities that determine the quality of the scheme. Thus, it is important to know how the theoretically predicted critical point τ_d^{I*} depends on the choice of σ_E, σ_I .

Although the critical point in the field model can be thought as a Hopf bifurcation point, the concept of critical point is not decisive in the E-I spiking neuronal network. This can be seen from Fig. 2C and Fig. S1B which show that the spiking correlation increases in a somewhat continuous way as τ_d^I increases. Furthermore, the critical properties of avalanche shown in Fig. 3 are statistical properties so that one can expect that for parameters close to the critical value these properties can still maintain in a statistically significant manner. As a first approximation, the critical point in the E-I spiking network can be defined as the parameter value where the distance of the avalanche size distribution to its best fit power law distribution, D defined in Methods, is minimal, as shown in Fig. 3C. We find that when σ_E, σ_I are estimated in the numerical way through Eq. (16), the critical point in the spiking network, is very close to the Hopf bifurcation point in the field model. We denote τ_d^{I*} as the Hopf bifurcation point in this ‘optimal’ estimation of the parameters σ_E, σ_I using Eq. (16).

We compute the Hopf bifurcation point $\tau_d^{I\text{Hopf}}(\sigma_E, \sigma_I)$ predicted by the field model for different values of σ_E, σ_I and compare it to the ‘real’ critical point (estimated by τ_d^{I*}). The difference $\tau_d^{I\text{Hopf}}(\sigma_E, \sigma_I) - \tau_d^{I*}$ of the CUB model and the COB model can be seen in Fig. S2. From Fig. S2, we can see that once σ_E, σ_I are estimated with suitable values, such as by Eq. (16) for CUB or COB models (white dots) or Eq. (15) for CUB model (black dots), the prediction of the critical synchronous transition point is very precise.

We also notice that the bifurcation point predict by the field model seems to mainly depend on the difference $\sigma_E - \sigma_I$. Once $\sigma_E - \sigma_I$ lies on suitable ranges, the predicted critical point will be very close to the ‘real’ one. It can also be noticed that in the CUB model the critical point is not sensitive to the values of σ_E, σ_I compared with the COB model, as can be seen from Fig. S2 A to C that the difference $\tau_d^{I\text{Hopf}}(\sigma_E, \sigma_I) - \tau_d^{I*}$ is still low for a large range of parameter values. This allows us to simply use Eq. (15) to estimate them. On the contrary, the sensitivity in the COB case implies that the COB model has more complicated intrinsic dynamic nature that has to be further explored.

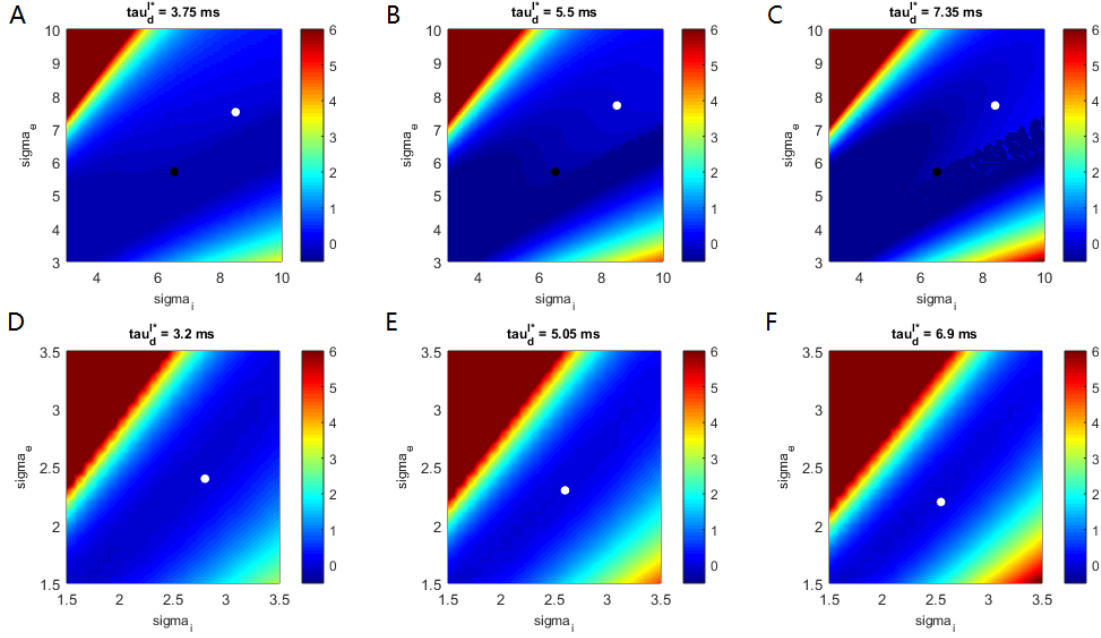


Fig. S2. Sensitivity of the predicted critical point on the effective parameters. The difference value $\tau_d^{I\text{Hopf}}(\sigma_E, \sigma_I) - \tau_d^{I*}$ is shown by color for current-based (CUB) model (A-C) and conductance-based (COB) model (D-F). White dots in (A-F) indicate the positions of the numerical estimation results by Eq. (16) and the corresponding estimated critical value τ_d^{I*} is shown on top of the plots. Black dots in (A-C) indicate the positions of the theoretical estimation results by Eq. (15) in the current-based model. Parameters are $\tau_d^E = 2\text{ ms}$ for (A, D), $\tau_d^E = 3\text{ ms}$ for (B, E), $\tau_d^E = 4\text{ ms}$ for (C, F) and $Q_o = 5\text{ Hz}$ for all the cases.

Supplementary table S1. Estimating the critical exponents of the data sets. The number of neurons, length of the up-states, the time bin used in measuring the avalanches, maximum avalanche size and duration, those estimated critical exponents, data ranges after truncations and the p-values in KS test of the fitted power laws in each data set are shown. Here, the avalanche size and duration are in their original linear scale.

Set No.	Neuron amounts	Up-state length (mins)	bin size (ms)	max size	max duratio	size range	τ	p value	duration range	α	p value	1/ovz	$(\alpha-1)/(\tau-1)$
1	166	12.60	3.70	627	162	[10,95]	1.78	0.118	[9,50]	2.183	0.108	1.218	1.226
2	443	28.24	2.05	476	115								
3	99	9.16	1.97	11502	1970	[4,125]	1.248	0.42	[4,52]	1.365	0.406	1.245	1.472
4	98	8.08	5.62	1713	264	[12,144]	1.223	0.18	[11,71]	1.349	0.516	1.223	1.565
5	367	11.35	3.53	1090	237	[7,124]	1.419	0.188	[4,25]	1.644	0.846	1.321	1.537
6	286	10.06	2.20	1798	365				[7,52]	1.442	0.88	1.271	
7	172	4.90	6.43	2230	245	[2,27]	1.837	0.984	[2,14]	2.088	0.804	1.327	1.300
8	191	8.06	2.19	8002	1304				[6,116]	1	0.644	1.204	
9	333	7.51	2.37	2775	677	[5,105]	1.751	0.212	[5,44]	1.95	0.878	1.309	1.265
10	368	17.56	2.44	1222	251				[9,59]	3.431	0.114	1.366	
11	243	16.79	1.25	2195	481								
12	346	14.45	1.03	1534	349				[7,50]	1.653	0.252	1.266	
13	381	16.40	1.34	1409	321	[7,116]	1.662	0.334	[4,33]	1.85	0.164	1.284	1.284
14	304	16.24	0.79	2071	450	[7,91]	1.452	0.226	[6,46]	1.599	0.22	1.248	1.325
15	206	16.49	1.07	2066	445	[7,90]	1.566	0.704					
16	594	22.72	0.87	1230	278								
17	435	10.07	2.75	1566	287	[7,113]	1.309	0.356	[3,24]	1.424	0.794	1.372	1.372
18	180	14.46	1.08	3280	525				[2,17]	1.621	0.146	1.310	
19	262	11.58	0.88	1685	407								
20	534	18.02	1.49	1318	273								
21	444	2.91	3.02	2985	334	[8,117]	1.377	0.806	[2,53]	1.5	0.978	1.326	1.326
22	384	20.85	0.76	2598	487								
23	310	13.79	1.14	5015	779								
24	358	12.33	1.08	2093	429				[13,100]	2.306	0.168	1.235	
25	231	10.71	1.93	3256	510	[5,150]	1.229	0.632					

Acknowledgments

This work was supported by the Hong Kong Baptist University (HKBU) Strategic Development Fund, the Hong Kong Research Grant Council (GRF12200217), the HKBU Research Committee and Interdisciplinary Research Clusters Matching Scheme 2018/19 (RC-IRCMs/18-19/SCI01) and the National Natural Science Foundation of China (Grants No. 11775314, No. 91530320 and No. 11975194). This research was conducted using the resources of the High-Performance Computing Cluster Centre at HKBU, which receives funding from the RGC and the HKBU.

References

1. Stringer C, Pachitariu M, Steinmetz N, Carandini M, Harris KD. High-dimensional geometry of population responses in visual cortex. *Nature*. 2019; 1.
2. Okun M, Steinmetz NA, Cossell L, Iacaruso M F, Ko H, Barthó P, et al. Diverse coupling of neurons to populations in sensory cortex. *Nature*. 2015;521: 511.
3. Stringer C, Pachitariu M, Steinmetz N, Reddy CB, Carandini M, Harris KD. Spontaneous behaviors drive multidimensional, brainwide activity. *Science* (80-). 2019;364: 255.
4. Holt GR, Softky WR, Koch C, Douglas RJ. Comparison of discharge variability in vitro and in vivo in cat visual cortex neurons. *J Neurophysiol*. 1996;75: 1806–1814.
5. Softky WR, Koch C. The highly irregular firing of cortical cells is inconsistent with temporal integration of random EPSPs. *J Neurosci*. 1993;13: 334–350.
6. Brunel N, Wang X-J. What determines the frequency of fast network oscillations with irregular neural discharges? I. Synaptic dynamics and excitation-inhibition balance. *J Neurophysiol*. 2003;90: 415–430.
7. Herrmann CS, Munk MHJ, Engel AK. Cognitive functions of gamma-band activity: memory match and utilization. *Trends Cogn Sci*. 2004;8: 347–355.
8. Beggs JM, Plenz D. Neuronal avalanches in neocortical circuits. *J Neurosci*. 2003;23: 11167–11177.
9. Gireesh ED, Plenz D. Neuronal avalanches organize as nested theta-and beta/gamma-oscillations during development of cortical layer 2/3. *Proc Natl Acad Sci*. 2008;105: 7576–7581.
10. Bellay T, Klaus A, Seshadri S, Plenz D. Irregular spiking of pyramidal neurons organizes as scale-invariant neuronal avalanches in the awake state. *Elife*. 2015;4: e07224.
11. Friedman N, Ito S, Brinkman BAW, Shimono M, DeVille REL, Dahmen KA, et al. Universal critical dynamics in high resolution neuronal avalanche data. *Phys Rev Lett*. 2012;108: 208102.
12. Shu Y, Hasenstaub A, McCormick DA. Turning on and off recurrent balanced cortical activity. *Nature*. 2003;423: 288.
13. Xue M, Atallah BV, Scanziani M. Equalizing excitation--inhibition ratios across visual

cortical neurons. *Nature*. 2014;511: 596.

14. Okun M, Lampl I. Instantaneous correlation of excitation and inhibition during ongoing and sensory-evoked activities. *Nat Neurosci*. 2008;11: 535.
15. Denève S, Machens CK. Efficient codes and balanced networks. *Nat Neurosci*. 2016;19: 375.
16. Abeles M. *Corticonics: Neural circuits of the cerebral cortex*. Cambridge University Press; 1991.
17. Schneidman E, Berry II MJ, Segev R, Bialek W. Weak pairwise correlations imply strongly correlated network states in a neural population. *Nature*. 2006;440: 1007.
18. Fontenele AJ, de Vasconcelos NAP, Feliciano T, Aguiar LAA, Soares-CunhaC, CoimbraB, et al. Criticality between cortical states. *Phys Rev Lett*. 2019;122: 208101.
19. Shew WL, Yang H, Yu S, Roy R, Plenz D. Information capacity and transmission are maximized in balanced cortical networks with neuronal avalanches. *J Neurosci*. 2011;31: 55–63.
20. Shew WL, Yang H, Petermann T, Roy R, Plenz D. Neuronal avalanches imply maximum dynamic range in cortical networks at criticality. *J Neurosci*. 2009;29: 15595–15600.
21. Kinouchi O, Copelli M. Optimal dynamical range of excitable networks at criticality. *Nat Phys*. 2006;2: 348.
22. Van Vreeswijk C, Sompolinsky H. Chaos in neuronal networks with balanced excitatory and inhibitory activity. *Science*. 1996;274: 1724–1726.
23. Van Vreeswijk C, Sompolinsky H. Chaotic balanced state in a model of cortical circuits. *Neural Comput*. 1998;10: 1321–1371.
24. Renart A, De La Rocha J, Bartho P, Hollender L, Parga N, Reyes A, et al. The asynchronous state in cortical circuits. *Science*. 2010;327: 587–590.
25. Landaul D, Egger R, Dercksen VJ, Oberlaender M, Sompolinsky H. The impact of structural heterogeneity on excitation-inhibition balance in cortical networks. *Neuron*. 2016;92: 1106–1121.
26. Litwin-Kumar A, Doiron B. Slow dynamics and high variability in balanced cortical networks with clustered connections. *Nat Neurosci*. 2012;15: 1498.
27. Wang S-J, Hilgetag C, Zhou C. Sustained activity in hierarchical modular neural networks: self-organized criticality and oscillations. *Front Comput Neurosci*. 2011;5: 30.
28. Rosenbaum R, Smith MA, Kohn A, Rubin JE, Doiron B. The spatial structure of correlated neuronal variability. *Nat Neurosci*. 2017;20: 107.
29. Darshan R, van Vreeswijk C, Hansel D. Strength of correlations in strongly recurrent neuronal networks. *Phys Rev X*. 2018;8: 31072.
30. Keane A, Gong P. Propagating waves can explain irregular neural dynamics. *J Neurosci*. 2015;35: 1591–1605.
31. Gu Y, Qi Y, Gong P. Rich-club connectivity, diverse population coupling, and dynamical

- activity patterns emerging from local cortical circuits. *PLoS Comput Biol*. 2019;15: e1006902.
32. Keane A, Henderson JA, Gong P. Dynamical patterns underlying response properties of cortical circuits. *J R Soc Interface*. 2018;15: 20170960.
 33. Yang D-P, Zhou H-J, Zhou C. Co-emergence of multi-scale cortical activities of irregular firing, oscillations and avalanches achieves cost-efficient information capacity. *PLoS Comput Biol*. 2017;13: e1005384.
 34. Salin PA, Prince DA. Spontaneous GABAA receptor-mediated inhibitory currents in adult rat somatosensory cortex. *J Neurophysiol*. 1996;75: 1573–1588.
 35. Zhou F-M, Hablitz JJ. AMPA receptor-mediated EPSCs in rat neocortical layer II/III interneurons have rapid kinetics. *Brain Res*. 1998;780: 166–169.
 36. Yang H, Shew WL, Roy R, Plenz D. Maximal variability of phase synchrony in cortical networks with neuronal avalanches. *J Neurosci*. 2012;32: 1061–1072.
 37. di Santo S, Villegas P, Burioni R, Muñoz MA. Landau-Ginzburg theory of cortex dynamics: Scale-free avalanches emerge at the edge of synchronization. *Proc Natl Acad Sci*. 2018;115: E1356–E1365.
 38. Dalla Porta L, Copelli M. Modeling neuronal avalanches and long-range temporal correlations at the emergence of collective oscillations: Continuously varying exponents mimic M/EEG results. *PLOS Comput Biol*. 2019;15: e1006924.
 39. Martinello M, Hidalgo J, Maritan A, DiSantoS, PlenzD, MuñozMA. Neutral theory and scale-free neural dynamics. *Phys Rev X*. 2017;7: 41071.
 40. Touboul J, Destexhe A. Power-law statistics and universal scaling in the absence of criticality. *Phys Rev E*. 2017;95: 12413.
 41. Poil S-S, Hardstone R, Mansvelder HD, Linkenkaer-Hansen K. Critical-state dynamics of avalanches and oscillations jointly emerge from balanced excitation/inhibition in neuronal networks. *J Neurosci*. 2012;32: 9817–9823.
 42. Lombardi F, Herrmann HJ, Perrone-Capano C, Plenz D, De Arcangelis L. Balance between excitation and inhibition controls the temporal organization of neuronal avalanches. *Phys Rev Lett*. 2012;108: 228703.
 43. Sethna JP, Dahmen KA, Myers CR. Crackling noise. *Nature*. 2001;410: 242.
 44. Ito S, Yeh F-C, Timme NM, Hottowy P, Litke AM, Beggs JM. Spontaneous spiking activity of hundreds of neurons in mouse somatosensory cortex slice cultures recorded using a dense 512 electrode array. *CRCNS org*. 2016.
 45. Churchland MM, Byron MY, Cunningham JP, Sugrue LP, Cohen MR, Corrado GS, et al. Stimulus onset quenches neural variability: a widespread cortical phenomenon. *Nat Neurosci*. 2010;13: 369.
 46. Teich MC, Heneghan C, Lowen SB, Ozaki T, Kaplan E. Fractal character of the neural spike train in the visual system of the cat. *JOSA A*. 1997;14: 529–546.
 47. Brunel N. Dynamics of sparsely connected networks of excitatory and inhibitory spiking neurons. *J Comput Neurosci*. 2000;8: 183–208.

48. Okun M, Lampl I. Balance of excitation and inhibition. *Scholarpedia*. 2009;4: 7467.
49. Yadav AC, Ramaswamy R, Dhar D. General mechanism for the $1/f$ noise. *Phys Rev E*. 2017;96: 22215.
50. di Santo S, Villegas P, Burioni R, Muñoz MA. Simple unified view of branching process statistics: Random walks in balanced logarithmic potentials. *Phys Rev E*. 2017;95: 32115.
51. Stevens CF, Zador AM. Input synchrony and the irregular firing of cortical neurons. *Nat Neurosci*. 1998;1: 210.
52. Haldeman C, Beggs JM. Critical branching captures activity in living neural networks and maximizes the number of metastable states. *Phys Rev Lett*. 2005;94: 58101.
53. Palva JM, Zhigalov A, Hirvonen J, Korhonen O, Linkenkaer-Hansen K, Palva S. Neuronal long-range temporal correlations and avalanche dynamics are correlated with behavioral scaling laws. *Proc Natl Acad Sci*. 2013;110: 3585–3590.
54. Mora T, Deny S, Marre O. Dynamical criticality in the collective activity of a population of retinal neurons. *Phys Rev Lett*. 2015;114: 78105.
55. Tkačik G, Mora T, Marre O, Amodei D, Palmer SE, Berry MJ, et al. Thermodynamics and signatures of criticality in a network of neurons. *Proc Natl Acad Sci*. 2015;112: 11508 LP – 11513. doi:10.1073/pnas.1514188112
56. Burkitt AN. A review of the integrate-and-fire neuron model: I. Homogeneous synaptic input. *Biol Cybern*. 2006;95: 1–19.
57. Ricciardi LM, Sacerdote L. The Ornstein-Uhlenbeck process as a model for neuronal activity. *Biol Cybern*. 1979;35: 1–9.
58. Fourcaud N, Brunel N. Dynamics of the firing probability of noisy integrate-and-fire neurons. *Neural Comput*. 2002;14: 2057–2110.
59. Shriki O, Hansel D, Sompolinsky H. Rate models for conductance-based cortical neuronal networks. *Neural Comput*. 2003;15: 1809–1841.
60. Renart A, Brunel N, Wang X-J. Mean-field theory of irregularly spiking neuronal populations and working memory in recurrent cortical networks. *Comput Neurosci A Compr approach*. 2004; 431–490.
61. Schaffer ES, Ostojic S, Abbott LF. A complex-valued firing-rate model that approximates the dynamics of spiking networks. *PLoS Comput Biol*. 2013;9: e1003301.
62. Augustin M, Ladenbauer J, Baumann F, Obermayer K. Low-dimensional spike rate models derived from networks of adaptive integrate-and-fire neurons: comparison and implementation. *PLoS Comput Biol*. 2017;13: e1005545.
63. Montbrió E, Pazó D, Roxin A. Macroscopic description for networks of spiking neurons. *Phys Rev X*. 2015;5: 21028.
64. Laing CR. Exact neural fields incorporating gap junctions. *SIAM J Appl Dyn Syst*. 2015;14: 1899–1929.
65. Dumont G, Gutkin B. Macroscopic phase resetting-curves determine oscillatory coherence and signal transfer in inter-coupled neural circuits. *PLoS Comput Biol*. 2019;15: e1007019.

66. Schwalger T, Deger M, Gerstner W. Towards a theory of cortical columns: From spiking neurons to interacting neural populations of finite size. *PLoS Comput Biol*. 2017;13: e1005507.
67. Mongillo G, Barak O, Tsodyks M. Synaptic theory of working memory. *Science* (80-). 2008;319: 1543–1546.
68. Levina A, Herrmann JM, Geisel T. Dynamical synapses causing self-organized criticality in neural networks. *Nat Phys*. 2007;3: 857.
69. Millman D, Mihalas S, Kirkwood A, Niebur E. Self-organized criticality occurs in non-conservative neuronal networks during up states. *Nat Phys*. 2010;6: 801.
70. Huang C, Ruff DA, Pyle R, Rosenbaum R, Cohen MR, Doiron B. Circuit models of low-dimensional shared variability in cortical networks. *Neuron*. 2019;101: 337–348.
71. Chaudhuri R, Knoblauch K, Gariel M-A, Kennedy H, Wang X-J. A large-scale circuit mechanism for hierarchical dynamical processing in the primate cortex. *Neuron*. 2015;88: 419–431.
72. Haimovici A, Tagliazucchi E, Balenzuela P, Chialvo DR. Brain organization into resting state networks emerges at criticality on a model of the human connectome. *Phys Rev Lett*. 2013;110: 178101.
73. Shelley MJ, Tao L. Efficient and accurate time-stepping schemes for integrate-and-fire neuronal networks. *J Comput Neurosci*. 2001;11: 111–119.
74. Dayan P, Abbott LF. Theoretical neuroscience: computational and mathematical modeling of neural systems. MIT press Cambridge, MA; 2001.
75. Wilson HR, Cowan JD. Excitatory and inhibitory interactions in localized populations of model neurons. *Biophys J*. 1972;12: 1–24.
76. Shriki O, Alstott J, Carver F, Holroyd T, Henson RNA, Smith ML, et al. Neuronal avalanches in the resting MEG of the human brain. *J Neurosci*. 2013;33: 7079–7090.
77. Benayoun M, Cowan JD, van Drongelen W, Wallace E. Avalanches in a stochastic model of spiking neurons. *PLoS Comput Biol*. 2010;6: e1000846.
78. Marsden JE, McCracken M. The Hopf bifurcation and its applications. Springer Science & Business Media; 2012.
79. Golomb D. Neuronal synchrony measures. *Scholarpedia*. 2007;2: 1347.
80. Cohen MR, Kohn A. Measuring and interpreting neuronal correlations. *Nat Neurosci*. 2011;14: 811.
81. Williams-Garcia RV, Beggs JM, Ortiz G. Unveiling causal activity of complex networks. *EPL (Europhysics Lett)*. 2017;119: 18003.
82. Marshall N, Timme NM, Bennett N, Ripp M, Lautzenhiser E, Beggs JM. Analysis of power laws, shape collapses, and neural complexity: new techniques and matlab support via the NCC toolbox. *Front Physiol*. 2016;7: 250.
83. Ito S, Yeh F-C, Hiolski E, Rydygier P, Gunning DE, Hottowy P, et al. Large-scale, high-resolution multielectrode-array recording depicts functional network differences of cortical

and hippocampal cultures. PLoS One. 2014;9: e105324.

84. Litke AM, Bezayiff N, Chichilnisky EJ, Cunningham W, Dabrowski W, Grillo AA, et al. What does the eye tell the brain?: Development of a system for the large-scale recording of retinal output activity. IEEE Trans Nucl Sci. 2004;51: 1434–1440.
85. Moreno-Bote R, Parga N. Role of synaptic filtering on the firing response of simple model neurons. Phys Rev Lett. 2004;92: 28102.
86. Richardson MJE, Gerstner W. Synaptic shot noise and conductance fluctuations affect the membrane voltage with equal significance. Neural Comput. 2005;17: 923–947.